netrin-1 dependence receptors. IMR32 cells were transfected with either a dominant-negative mutant for DCC (DN-DCC) or UNC5H (DN-UNC5H) proapoptotic activity. These dominant-negative mutants of dependence receptors actually encode the intracellular domain of these receptors mutated in their caspase cleavage sites, and these mutants have been shown both in vitro and in vivo to specifically block the proapoptotic activity of their wild-type counterparts (3, 9, 33). Cell death was then analyzed after netrin-1 inhibition by siRNA. Although DN-DCC expression failed to inhibit netrin-1 siRNA-induced IMR32 cell death, expression of DN-UNC5H rendered IMR32 cells resistant to netrin-1 siRNA (Fig. 5 A). To more formally exclude the role in this death process of DCC or of altered forms of DCC that are known to be expressed in IMR32 cells (Fig. S2 C) (34), DCC was down-regulated by a siRNA approach and cell death was induced via netrin-1 siRNA. As shown in Fig. 5 B, DCC siRNA had no effect on cell death per se and failed to inhibit netrin-1 siRNA-induced caspase-3 activation, strengthening the perception that in these cells DCC is not proapoptotic. Neogenin, a DCC homologue, has also been proposed to act as a receptor for netrin-1 (35, 36) even though this is still a matter of controversy (5, 37). We then investigated whether neogenin, which is expressed in IMR32 cells (Fig. S2 C), could be implicated in the IMR32 cell death observed here. Neogenin was down-regulated by a siRNA approach and, as shown in Fig. S3 A, this has no effect on netrin-1 siRNA-mediated IMR32 cell death. Thus, the netrin-1 autocrine loop probably blocks UNC5H-induced IMR32 cell death.

To more specifically address the identity of the UNC5H receptors involved in this cell death induction, we down-regulated the expression of each UNC5H receptor individually (UNC5H1, UNC5H2, UNC5H3, or UNC5H4) by a siRNA approach (Fig. 5 C and Fig. S3 B) while inducing cell death using netrin-1 siRNA (Fig. S3 C). None of the single UNC5H siRNAs was sufficient to inhibit netrin-1 siRNA-mediated IMR32 cell apoptosis, suggesting some redundancy in UNC5H-induced cell death (Fig. 5 D). However, when combinations of siRNAs were used, we observed that combined silencing of the four UNC5H receptors was sufficient to fully inhibit the death triggered by netrin-1 autocrine loop disruption (Fig. 5 D), whereas the same combination of siRNAs had no effect on CLB-Ge2 cell survival (Fig. S3 D). The respective importance of UNC5H receptors in netrin-1 siRNA-induced cell death was then assessed by the different combination of two or three siRNAs; the combination of UNC5H1, UNC5H3, and UNC5H4 siRNAs was the only one to fully block cell death (Fig. 5 E). Thus, in agreement with the level of UNC5H receptors expressed in IMR32 cells, it appears that disruption of the netrin-1 autocrine survival loop triggers UNC5H-induced cell death. Moreover,

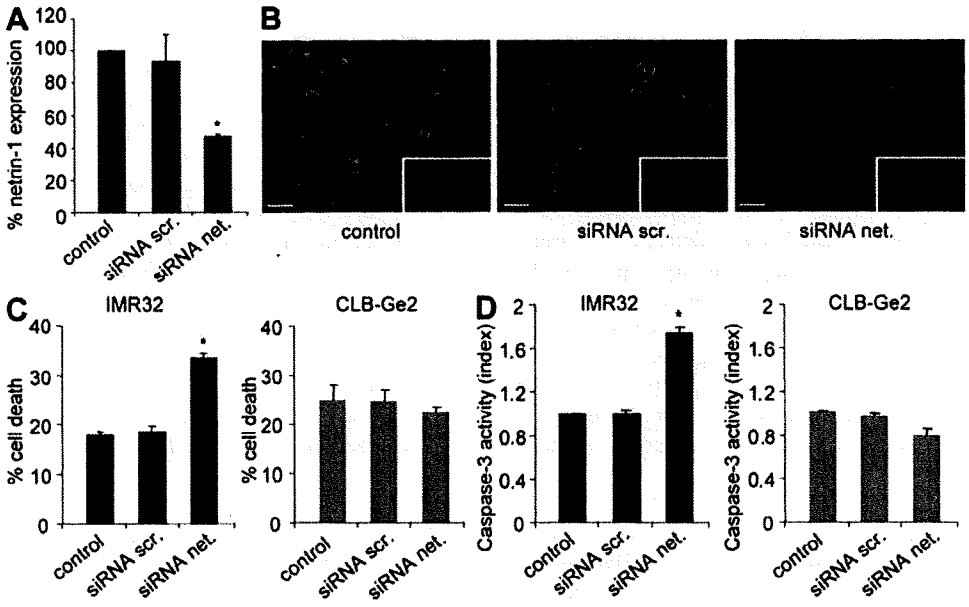

Figure 3. Down-regulation of netrin-1 autocrine loop by siRNA triggers NB tumor cell death. (A) Analysis of netrin-1 expression using Q-RT-PCR in nontransfected (control) IMR32 cell line or 24 h after transfection with scramble siRNA (siRNA scr.) or with netrin-1 siRNA (siRNA net.). Data are means of three independent experiments. Error bars indicate SEM. *, $P < 0.05$ using a two-sided Mann-Whitney test compared with levels in control. (B) Immunostaining on IMR32 cell line using netrin-1 antibody in the absence of transfection (control) or 24 h after transfection with scramble siRNA or netrin-1 siRNA. Note that the general caspase inhibitor z-VAD-fmk was added to avoid cell death induced by netrin-1 siRNA. Insets show control without primary antibody. Bars, 50 μm. (C and D) Cell death induction in IMR32 and CLB-Ge2 cell lines was quantified in nontransfected cells (control) or after transfection with either scramble siRNA or netrin-1 siRNA using trypan blue exclusion assay (C) or relative caspase-3 activity assay (D). Data are means of four independent experiments. In C and D, error bars indicate SEM. *, $P < 0.05$ calculated using a two-sided Mann-Whitney test compared with level of control.

UNC5H1, UNC5H3, and UNC5H4 are the receptors involved in this proapoptotic effect.

Furthermore, in IMR32 cells, the proapoptotic serine threonine kinase DAP kinase (DAPK), which is shown to be required for UNC5H-induced cell death, exhibited a loss of its inhibitory autophosphorylation (38) upon DCC-5Fbn treatment (Fig. 5 F) or netrin-1 siRNA transfection (Fig. 5 G). Accordingly, autophosphorylation was restored by a treatment with excess netrin-1 or by a combination of UNC5H1, UNC5H3, and UNC5H4 siRNAs. Moreover, the transfection of the antiapoptotic protein BCL-2 was sufficient to inhibit netrin-1 siRNA-induced cell death but did not inhibit DAPK dephosphorylation, hence suggesting that DAPK activation is not a result of cell death but is specifically engaged by UNC5H after netrin-1 inhibition (unpublished data).

Interference with netrin-1 inhibits NB progression and dissemination

We next assessed whether in vivo modulation of netrin-1 could be used to limit/inhibit NB progression and dissemination. An elegant chicken model has been developed in which graft of NB cells in the chorioallantoic membrane (CAM) of 10-d-old chick embryos recapitulates both tumor growth at a primary site, i.e., within the CAM, and tumor invasion and dissemination at a secondary site, metastasis to the lung (Fig. 6 A). In a first approach, IMR32 or CLB-Ge2 cells were loaded in

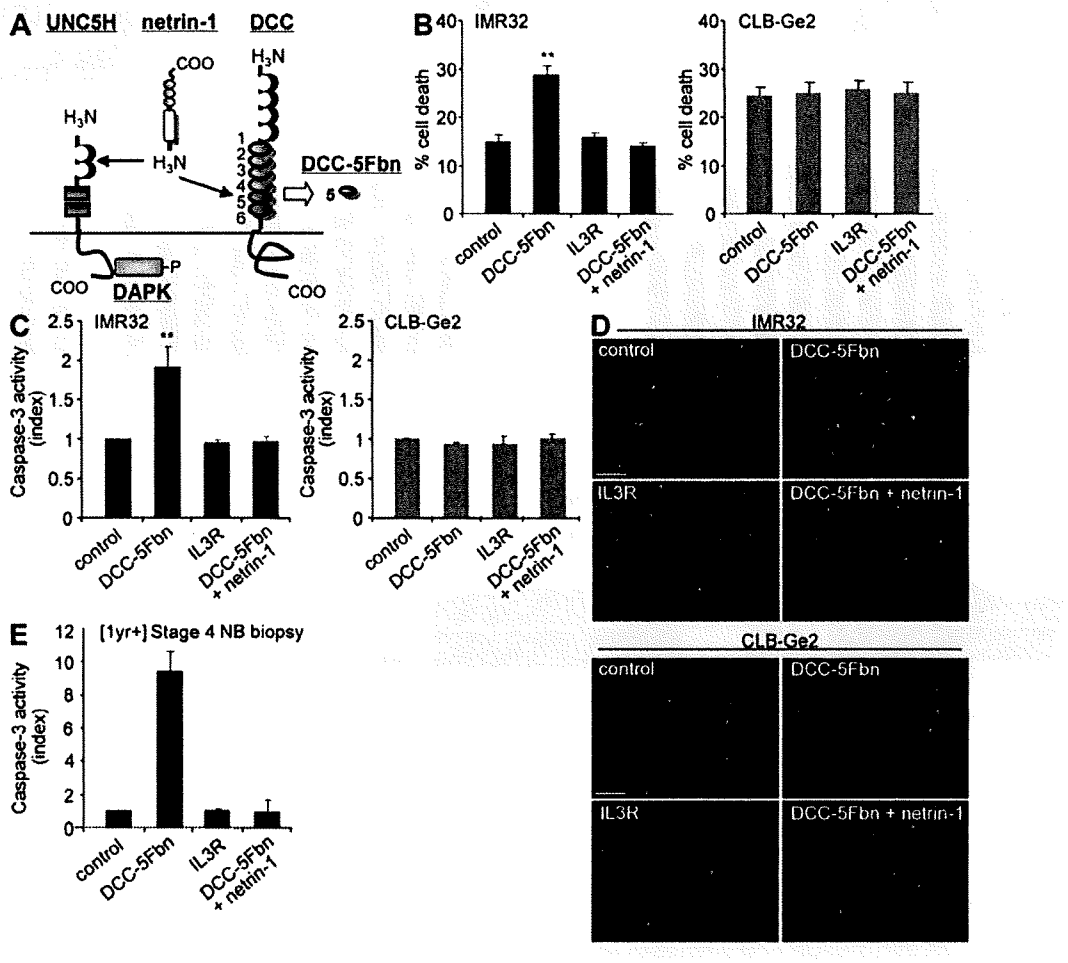

Figure 4. Disruption of netrin-1 autocrine loop by a decoy receptor fragment triggers NB tumor cell death. (A) Scheme representing netrin-1 and its receptors DCC and UNC5H and the fifth fibronectin type III domain of DCC (DCC-5Fbn) used to induce cell death. The downstream effector DAPK implicated in UNC5H-induced cell death is also represented. (B–D) Quantitative analysis of cell death in IMR32 and CLB-Ge2 cell lines treated with 1 μg/ml DCC-5Fbn, with or without addition of netrin-1 in excess (150 ng/ml) to reverse the effect of DCC-5Fbn. A negative control was also performed by adding an unrelated IL3R peptide produced in the same condition as DCC-5Fbn. Cell death was quantified by trypan blue exclusion assay (B) while apoptosis was monitored by measuring relative caspase-3 activity (C) or by TUNEL staining (D). Bars, 100 μm. In D, TUNEL staining was performed on three independent experiments. (E) Effect of DCC-5Fbn on fresh [1yr+] stage 4 NB. Tumoral cells were directly resuspended from the surgical punction and were plated for 24 h in presence of treatment. In B and C, data are means of six independent experiments. In E, data are means of two independent experiments. Error bars indicate SEM. **, $P < 0.01$ calculated using a two-sided Mann-Whitney test compared with level of control.

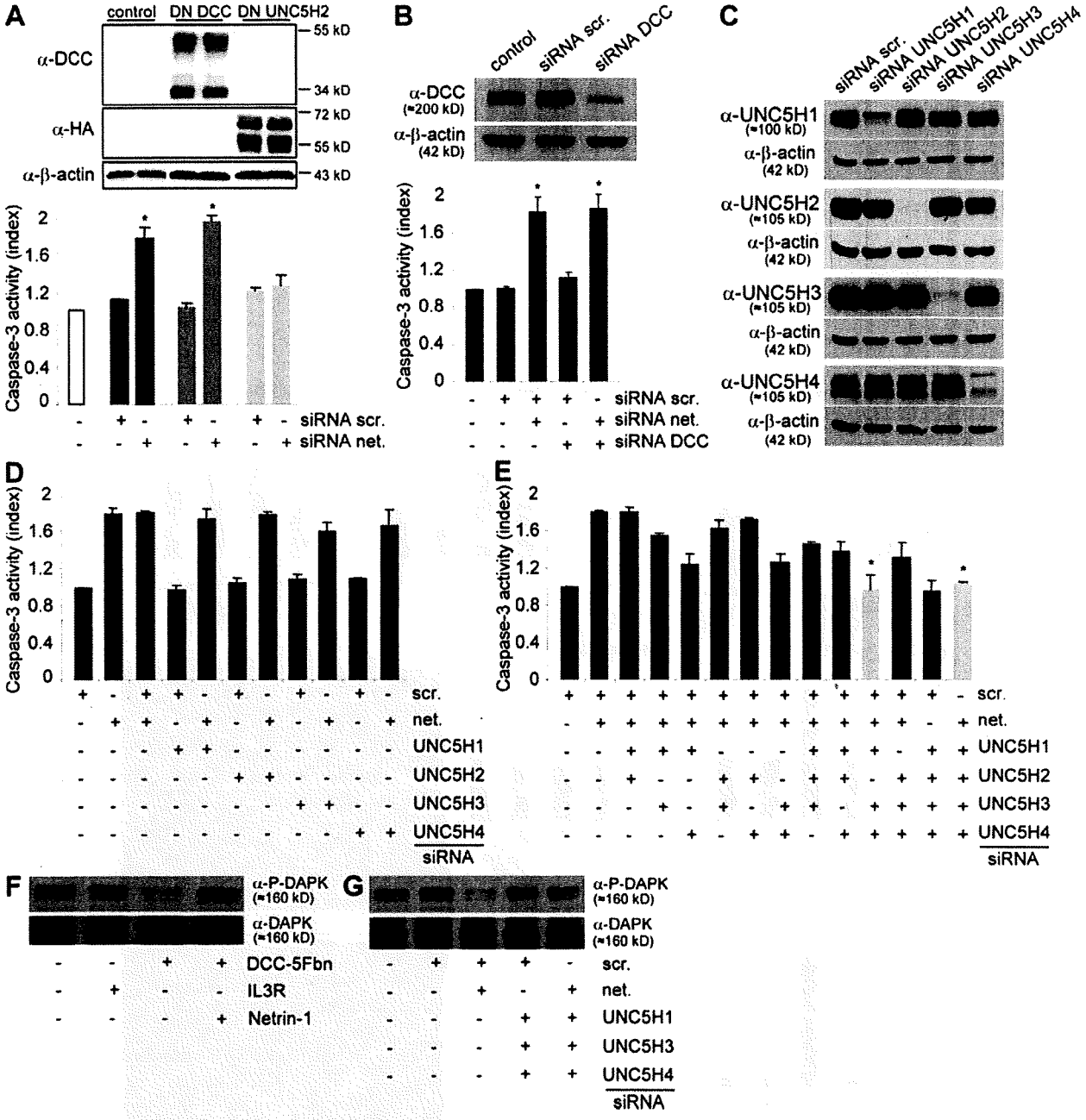

Figure 5. NB tumor cell death occurs via UNC5H/DAPK proapoptotic signaling. (A) Quantification of cell death in IMR32 cells transfected with either a dominant-negative mutant for DCC proapoptotic activity (DN-DCC) or a dominant-negative mutant for UNC5H proapoptotic activity (DN-UNC5H). Top: DN-DCC and DN-UNC5H proteins expression were analyzed by Western blot. Bottom: cell death was quantified by measuring relative caspase-3 activity after scramble or netrin-1 siRNA transfection. SEM are indicated. Data are means of three independent experiments. *, $P < 0.05$ calculated using a two-sided Mann-Whitney test compared with level of control. (B) Quantification of cell death in IMR32 cells transfected with either a scramble siRNA or a netrin-1 siRNA together or not with a DCC siRNA. Top: DCC siRNA efficiency was verified by Western blotting on HEK293T cells transfected with pCR-hDCC together with scramble or DCC siRNA. Bottom: cell death was quantified by measuring relative caspase-3 activity. Data are means of three independent experiments. SEM are indicated. *, $P < 0.05$ calculated using a two-sided Mann-Whitney test compared with level of control. Similar results were obtained when neogenin or MYCN were down-regulated (Fig. S3 A). (C) Analysis of specificity and efficiency of each UNC5H siRNA by Western blot in HEK293T cells transfected with UNC5H1, H2, H3, or H4 encoding vector together with each UNC5H siRNA. (D and E) Quantification of cell death in IMR32 cells transfected with either a scramble siRNA or a netrin-1 siRNA together with various combinations of UNC5H siRNA, i.e, one UNC5H (D) or two or four UNC5H (E). Apoptosis was monitored by measuring relative caspase-3 activity. The use of combined UNC5H1, UNC5H2, UNC5H3, and

10-d-old CAM and embryos were treated on days 11 and 14 with PBS or DCC-5Fbn. 17-d-old chicks were then analyzed for primary tumor growth and metastasis to the lung. As shown in Fig. 6 (B and C), specifically in CAMs grafted with IMR32 but not with CLB-Ge2 cells, DCC-5Fbn significantly reduced primary tumor size. This size reduction was associated with increased tumor apoptosis, as shown by an increased caspase-3 activity in the tumor lysate (Fig. 6 D). More importantly, DCC-5Fbn also reduced lung metastasis formation, as shown in Fig. 6 E. Similar results were obtained when CAM-grafted embryos were treated with netrin-1 siRNA (unpublished data). To next assess whether DCC-5Fbn could also induce the regression of metastatic lesions, IMR32 cells were CAM grafted and DCC-5Fbn (or PBS) treatment started after metastasis to the lung is known to occur, i.e., treatments were performed on days 14 and 15 because pulmonary metastases are routinely detectable at day 13. As shown in Fig. 6 F, pulmonary metastases were markedly reduced, suggesting that DCC-5Fbn not only inhibits tumor dissemination but also induces regression of metastatic lesions at the secondary site.

As a second in vivo approach, we used the IGR-N-91 model derived from a BM metastasis of human MYCN-amplified stage 4 NB. When subcutaneously xenografted into nude mice, IGR-N-91 cells gave rise to different tumor cell lines derived from the *nude* mouse primary tumor xenograft (PTX) or from disseminated metastatic foci into BM, blood, and myocardium (Myoc) of the animal (39). It is of interest that although the parental IGR-N-91 and the cell line derived from the PTX show no or very low netrin-1 expression, the different cell lines derived from secondary localizations showed a marked expression of netrin-1 both at the RNA level (Fig. 7 A) and at the protein level (Fig. 7 B). When cell death was investigated in these different cell lines upon treatment with DCC-5Fbn, a direct correlation was observed between the level of netrin-1 and cell susceptibility to DCC-5Fbn (Fig. 7 C). Specifically, although PTX cells failed to undergo cell death upon DCC-5Fbn treatment, this treatment triggered netrin-1–high Myoc cell death (Fig. 7 C). This observation supports the overall view that gaining netrin-1 dependence receptor resistance, via an autocrine netrin-1 expression in the case of the IGR-N-91 model, likely promotes NB tumor cell survival outside of the primary tumor site. To test whether this netrin-1 expression may then be used as a target to inhibit metastasis in vivo, Myoc and PTX cells were injected intravenously into *nude* mice and lung colonization was quantitated after daily intraperitoneal treatment with PBS or DCC-5Fbn. Although lung colonization was not reduced upon DCC-5Fbn treatment in PTX-injected mice (not depicted), a significant decrease in lung colonization was detected in DCC-5Fbn–treated Myoc-injected mice (Fig. 7 D). Thus, in both chick and mouse models, disruption of the netrin-1 autocrine loop inhibited or completely prevented the dissemination of netrin-1–expressing NB cells.

DISCUSSION

Together, the data obtained in the chick and mouse models described in the previous sections, in NB cell lines, and in the human pathology all support the view that a fraction of NB shows an autocrine production of netrin-1. This elevated netrin-1 level likely confers a selective advantage acquired by the cancer cell to escape netrin-1 dependence receptor–induced apoptosis and, consequently, to survive in settings of environmental absence or limitation of netrin-1. It is therefore interesting to note that not only NB but also other neoplasms associated with poor prognosis, for example, metastatic breast cancer and pancreatic cancer, also express high levels of netrin-1 (33, 40), suggesting that netrin-1 up-regulation may be a common feature for several aggressive cancers. From a mechanistic point of view, in a large fraction of NB, this autocrine expression of netrin-1 probably inhibits UNC5H-induced cell death. However, because DCC has been shown to display reduced expression in NB and because this reduction has been associated with NB aggressiveness in human NB (29), it is tempting to speculate that netrin-1 up-regulation can also, in some NB, inhibit DCC-induced apoptosis. Interestingly, this netrin-1 up-regulation appears to block a death signal involving the serine threonine DAPK, whose activity is regulated via its autophosphorylation. It is therefore of interest to note that DAPK was described to be a negative regulator of tumor progression and, more specifically, of metastasis (41). Thus, it can be suggested that a fraction of low netrin-1–expressing NB may have selected a loss of function of DAPK for survival. This would be compatible with the finding that metastasis in NB is associated with a loss of caspase-8, a selective advantage which provides survival to NB cells by inhibiting the proapoptotic signaling of the dependence receptor integrin $\alpha 3\beta 1$ (42).

It is then interesting to wonder why such a large fraction of aggressive NBs have selected a gain of netrin-1 rather than a loss of the netrin-1 dependence receptor death pathways. A possible explanation is that netrin-1 expression not only confers a gain in survival, but may also lead to enhancement of non-apoptotic signaling mediated by netrin-1 receptors. Netrin-1 was indeed shown to bind a complex that includes some integrins (43). These integrins regulate cell migration and invasiveness and, thus, may play a role in cancer progression. Netrin-1 was also proposed to play a role in angiogenesis, although whether netrin-1 is proangiogenic or antiangiogenic is controversial (44–47) and this effect on angiogenesis may increase NB metastases development. It is also of interest to note that NB is a complex disease that originates from migrating neural crest cells. Netrin-1 up-regulation may then be implicated in

UNC5H4 or UNC5H1, UNC5H3, and UNC5H4 siRNAs, leading to the absence of death induced by netrin-1 siRNA, are presented in gray. Data are means of three independent experiments. Error bars indicate SEM. *, $P < 0.05$ calculated using a two-sided Mann-Whitney test compared with level of control. (F and G) Immunodetection of phosphorylated DAPK (P-DAPK) in IMR32 cells either treated with DCC-5Fbn (F) or transfected with netrin-1 siRNA alone or with UNC5H1, H3, and H4 siRNAs (G). In F and G, immunodetection was performed on three independent experiments.

the main function played by netrin-1 during nervous system development that is neuronal navigation. Along this line, netrin-1 and DCC have been shown to play an important role during neural crest cell migration (48), and it is then tempting to suggest that the gain in netrin-1 expression also promotes NB cell migration.

As different types of stage 4 NBs are distinguished, not only by the age of the children but also by the tissues in which metastases are found, one may wonder about the implication of netrin-1 produced in the normal tissues in which the tumor cells spread, and this would be interesting to explore. In particular, it would be interesting to evaluate whether, according to the classical "seed and soil" theory for metastasis (for review see reference 18), netrin-1 expression in specific tissues may favor metastasis development more specifically in these tissues. It is also intriguing

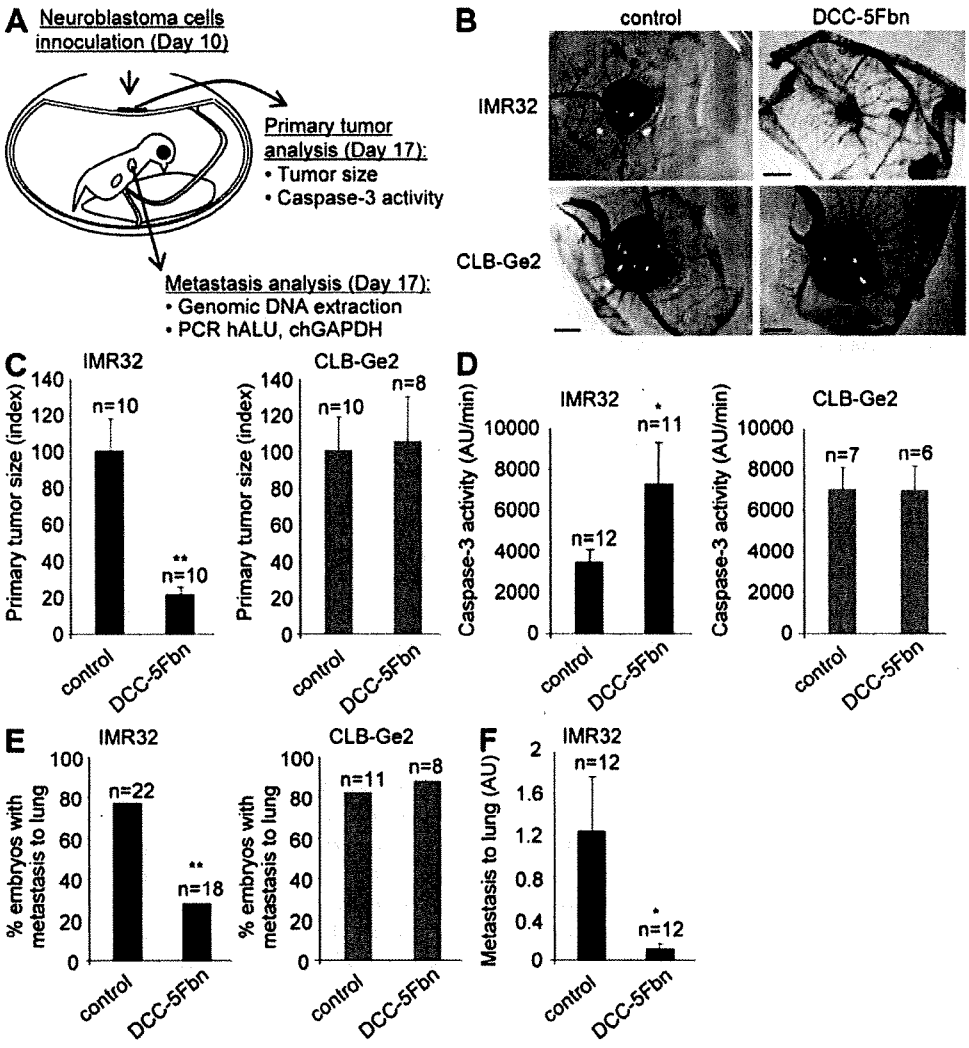

Figure 6. Disruption of netrin-1 autocrine loop inhibits NB progression and dissemination in a chick model. (A) Schematic representation of the experimental chick model. IMR32 or CLB-Ge2 cells were grafted in CAM at day 10 and DCC-5Fbn or PBS was injected on days 11 and 14. Tumors and lungs were harvested on day 17. (B–D) Effect of DCC-5Fbn on primary tumor growth and apoptosis. (B) Representative images of IMR32 (top) or CLB-Ge2 (bottom) primary tumors formed on CAM treated either with DCC-5Fbn (right) or PBS (left). Bars, 2 mm. (C) Quantitative analysis showing the mean primary tumor size. (D) Caspase-3 activity was determined in the primary tumor lysates from DCC-5Fbn/PBS-treated IMR32 or CLB-Ge2–grafted embryos. (E) Effect of DCC-5Fbn on lung metastasis. Percentage of embryos with lungs invaded by human IMR32 or CLB-Ge2 cells after two injections (days 11 and 14) of either DCC-5Fbn or PBS was performed as described in the Materials and methods. (F) Effect of DCC-5Fbn on lung metastasis regression. Quantification of lung metastasis in embryos CAM grafted with IMR32 cells and treated after metastasis formation (days 14 and 15) with DCC-5Fn or PBS. The number of embryos studied in each condition is indicated above the graphs and results are from three independent experiments. In C–F, errors bars indicate SEM. C–F: *, $P < 0.05$; **, $P < 0.005$ calculated using a two-sided Mann-Whitney test compared with level of control. E: **, $P < 0.005$ calculated using a Chi-squared test.

to note that others have shown that in some particular cell lines, netrin-1 is able to promote apoptosis rather than inhibit apoptosis (49), so that the view of netrin-1 up-regulation being only a survival-selective advantage to block apoptosis via dependence receptors is probably only part of the overall regulatory mechanisms that links NB, netrin-1, and its receptors.

The observation that low levels of netrin-1 in NB correlate with good outcome is of clinical interest, in particular in NB diagnosed in neonates and infants. Indeed, low netrin-1 expression predicts long-term survival in infants (100% in 4S stage and 90% in infants in general) in a type of pathology in which therapeutic management is highly dependent on presentation and MNA (50, 51). This is particularly true with

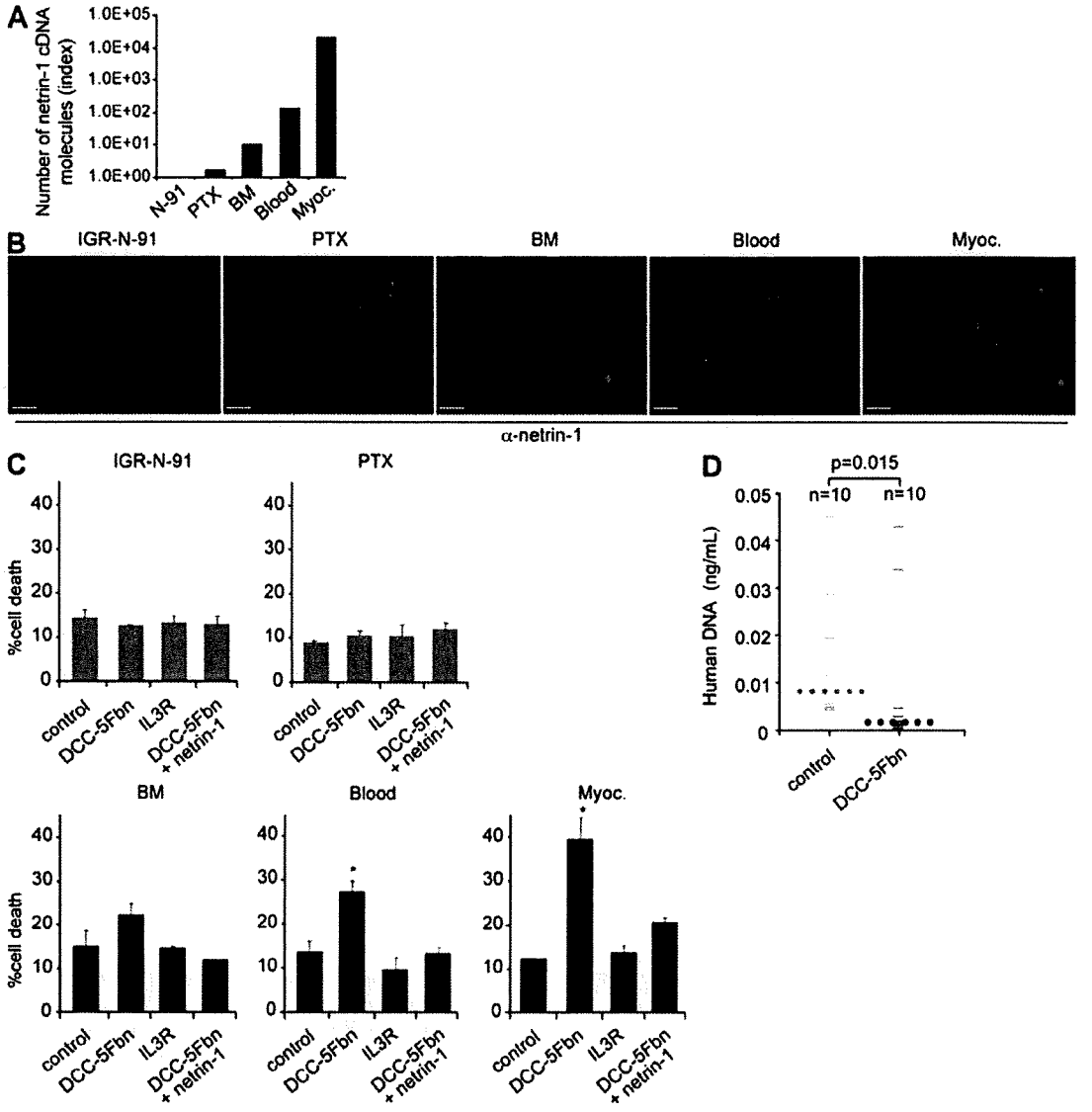

Figure 7. Disruption of netrin-1 autocrine loop inhibits NB dissemination in a mouse model. (A) Analysis of netrin-1 expression using Q-RT-PCR in IGR-N-91 cell line and the IGR-N-91-derived cell lines PTX, BM, Blood, and Myoc. Note that although PTX cells fail to express netrin-1, netrin-1 mRNA is highly expressed in Myoc cells. (B) Immunostaining on IGR-N-91 cells and the different derived cell lines PTX, BM, Blood, or Myoc using netrin-1 antibody. Bar, 50 µm. (C) Cell death was quantified in IGR-N-91, PTX, BM, Blood, or Myoc cell lines treated or not with DCC-5Fbn, with or without addition of netrin-1 in excess to reverse the effect of DCC-5Fbn. A negative control was also performed by adding an unrelated IL3R peptide produced in the same condition as DCC-5Fbn. Data are means of three independent experiments. Errors bars indicate SEM. *, $P < 0.05$, calculated using a two-sided Mann-Whitney test compared with level of control. (D) Quantification of lung colonization in PTX or Myoc cells in i.v injected mice treated with PBS or DCC-5Fbn for 22 d. Quantification was performed as described in the Materials and methods. Large bars indicate the median values for both groups. P-value was calculated using a two-sided Mann-Whitney test compared with level of control.

stage 4S infants who receive no (or minimal) treatment based on the lack of MNA, even though current statistics show that 1 in 10 of these infants will eventually die of NB. In this paper, we propose that determination of low netrin-1 level confirms a good prognosis for these infants without therapy, whereas the infants with high netrin-1 expression should be considered for more intensive treatment. Regarding infants or children with high netrin-1–expressing NB tumors, an alternative or supplementary targeted treatment based on disruption of the netrin-1 autocrine survival loop may improve standard high-dose chemotherapy regimen efficiency. We propose that a treatment based on inhibition of the interaction between netrin-1 and its dependence receptors, or inhibition of the ability of netrin-1 to multimerize its receptors, could potentially improve the survival of a large fraction of the patients suffering from aggressive NB. Moreover, it is interesting to note that no correlation between netrin-1 upregulation and molecular signature of apoptosis and invasion was observed in NB tumors (Fig. S1 D), strengthening the case for netrin-1 as an original target for NB. Future preclinical and clinical studies should assess whether such therapeutic strategies, which could include small molecules (drugs), monoclonal antibodies, or the DCC-5Fbn recombinant protein presented in this paper, used alone or in combination with standard chemotherapy, could be of therapeutic benefit for infants and children with NB.

MATERIALS AND METHODS

Cell lines, transfection procedure, and reagents. Human NB cell lines were obtained from the tumor banks at Centre Léon Bérard and at Institut Gustave Roussy. More specifically, IMR32 and CLB-Ge2 cell lines were cultured in RPMI 1640 GlutaMAX medium (Invitrogen) containing 10% FBS. IGR-N-91 cell line and its derivatives, as well as HEK293T cells, were cultured in DME medium (Invitrogen) containing 10% FBS. Cell lines were transfected using Lipofectamine 2000 reagent (Invitrogen) for siRNA or Lipofectamine Plus reagent (Invitrogen) for plasmids. Netrin-1 was obtained from Axxora and was used at a concentration of 150 ng/ml in all in vitro assays.

Human NB tumor samples and biological annotations. According to parental consent, surgical human NB tumor material was immediately frozen. Material and annotations were obtained from the Biological Resources Centers of both national referent Institutions for NB treatment (Centre Léon Bérard and at Institut Gustave Roussy). Protocols using human material were approved by the local ethics Committees of Lyon University and Paris XI University. MYCN genomic content was assessed on histologically qualified tumors as previously described (52). For immunohistochemistries, 5-µm sections were prepared and frozen at −80°C.

Plasmid constructs, siRNA, and DCC-5Fbn production. The dominant-negative mutant for UNC5H and DCC (pCR-UNC5H2-IC-D412N and pCR-DCC-IC-D1290N, respectively) and the plasmids encoding Neogenin (pCDNA3-Neogenin) and UNC5H1 (pCDNA3.1-UNC5H1-HA) have been previously described (1, 2, 5). The plasmids encoding UNC5H2 (pCDNA3.1-UNC5B-HA), UNC5H3 (pCDNA3-UNC5C-HA), and UNC5H4 (pCAG3-hU5H4-His) were gifts from H. Arakawa (National Cancer Institute, Tokyo, Japan), M. Tessier-Lavigne (Genentech, San Francisco, CA), K.L. Guan (University of Michigan, Ann Arbor, MI), and N. Yamamoto (Osaka University, Osaka, Japan). Human netrin-1–encoding plasmid (peak8-hNTN1-His) was obtained from D.E. Bredesen (The Buck Institute for Age Research, Novato, CA). Ps974-DCC-5Fbn allowing bacterial expression of the fifth fibronectin type III domain of DCC was obtained by inserting a Pst1–BamH1 DNA fragment generated by PCR using pDCC-CMV-S as a template. DCC-5Fbn production was performed using a standard procedure. In brief, BL21 cells were forced to express DCC-5Fbn in response to imidazole, and the BL21 lysate was subjected to affinity chromatography using FLAG-Sepharose (Sigma-Aldrich). A peptide corresponding to the ectodomain of IL3R was produced in the same conditions and used as a control. For cell culture use, netrin-1, DCC, and neogenin siRNAs (Santa Cruz Biotechnology, Inc.) were designed as a pool of three target-specific 20–25-nt siRNAs. UNC5H1, UNC5H2, UNCH3, and UNC5H4 siRNAs were designed by Sigma-Aldrich. MYCN siRNA was designed by Thermo Fisher Scientific.

Cell death assays. 2×10^5 cells were grown in serum-poor medium and were treated (or not) with 1 µg/ml DCC-5Fbn or transfected with siRNA using Lipofectamine 2000. Cell death was analyzed using trypan blue staining procedures as previously described (1). The extent of cell death is presented as the percentage of trypan blue–positive cells in the different cell populations. Apoptosis was monitored by measuring caspase-3 activity as described previously (1) using the Caspase 3/CPP32 Fluorimetric Assay kit (Gentaur). For detection of DNA fragmentation, treated cells were cytospun, and TUNEL was performed with 300 U/ml TUNEL enzyme and 6 µM biotinylated dUTP (Roche) as previously described (53).

Q-RT-PCR. To assay netrin-1, DCC, and UNC5H receptor expression in NB samples, total RNA was extracted from histologically qualified tumor biopsies (>60% immature neuroblasts) using the NucleoSpin RNAII kit (Macherey-Nagel), and 200 ng were reverse transcribed using 1U Superscript II reverse transcription (Invitrogen), 1U RNase inhibitor (Roche), and 250 ng of random hexamer (Roche). Total RNA was extracted from mouse and human cell lines using the NucleoSpin RNAII kit and 1 µg was reverse transcribed using the iScript cDNA Synthesis kit (Bio-Rad Laboratories). Real-time Q-RT-PCR was performed on a LightCycler 2.0 apparatus (Roche) using the LightCycler FastStart DNA Master SYBER Green I kit (Roche). Reaction conditions for all optimal amplifications, as well as primer selection for murine and human netrin-1, DCC, and UNC5H1-4, were determined as already described. The ubiquitously expressed human HPRT genes showing the least variability in expression in NB was used as an internal control (54). The sequences of the primers are the following: NTN1, 5′-TGCAAGAAGGACTATGCCGTC-3′ and 5′-GCTCGTGCCCTGCTTATACAC-3′; UNC5H1, 5′-CATCACCAAGGACACAAGGTTTGC-3′ and 5′-GGCTGGAAATTATCTTCTGCCGAA-3′; UNC5H2, 5′-GGGCTGGAGGATTACTGGTG-3′ and 5′-TGCAGGAGAACCTCATGGTC-3′; UNC5H3, 5′-GCAAATTGCTGGCTAAATATCAGGAA-3′ and 5′-GCTCCACTGTGTTCAGGCTAAATCTT-3′; UNC5H4, 5′-GGTGAACCCAGCCTCCAGTCAG-3′ and 5′-CTTCCACTGACATCACTTCCTCCC-3′; DCC, 5′-AGCCAATGGGAAAATTACTGCTTAC-3′ and 5′-AGGTTGAGATCCATGATTTGATGAG-3′; and HPRT, 5′-TGACACTGGCAAAACAATGCA-3′ and 5′-GGTCCTTTTCACCAGCAAGCT-3′.

Genomic DNA quantification. Genomic DNA from IMR32 and CLB-Ge2 cells was extracted with the NucleoSpin Tissue kit (Macherey-Nagel). 50 ng of genomic DNA was used to perform quantitative PCR using primers specific to *NTN1* and *MYCN* genomic sequences. Real-time quantitative PCR was performed on a LightCycler 2.0 apparatus using the Light Cycler FastStart DNA Master SYBER Green I kit. *NAGK* (the *N*-acetylglucosamine kinase gene), which is located on chromosome 2 similarly to the *MYCN* gene but separated from the MYCN amplicon, was used as an internal control gene to determine the gene dosage (55). For each pair of primers, genomic DNA amplification was assessed by polymerase activation at 95°C for 10 min, followed by 35 cycles at 95°C for 10 s, 65°C for 30 s, and 72°C for 10 s. The sequences of the primers are the following: *NTN1*, 5′-CTGTGTCCCCCACTTGTTCT-3′ and 5′-CCATGAACCCCACTGACTCT-3′; *MYCN*, 5′-GTGCTCTCCAATTCTCGCCT-3′ and 5′-GATGGCCTAGAGGAGGGCT-3′; and *NAGK*, 5′-TGGGCAGACACATCGTAGCA-3′ and 5′-CACCTTCACTCCCACCTCAAC-3′.

Immunohistochemistry and immunoblotting analysis. 10^5 cells were centrifugated on coverslips with a cytospinner (Shandon Cytospin 3; Thermo Fisher Scientific). Tumor slides and cells were fixed in 4% paraformaldehyde. The slides were then incubated at room temperature for 1 h with an antibody recognizing the human netrin-1 (1:150; R&D Systems), UNC5H1 (1:100; Abcam), UNC5H3 (1:100; R&D system), or UNC5H4 (1:100; Santa Cruz Biotechnology, Inc.). After rinsing in PBS, the slides were incubated with an Alexa 488 donkey anti–rat antibody (Invitrogen), an Alexa 488 donkey anti–rabbit antibody (Invitrogen), a Cy3 donkey anti–mouse antibody (Jackson ImmunoResearch Laboratories), or an Alexa 488 donkey anti–goat antibody (Invitrogen), respectively. For tumor slides, netrin-1 and UNC5H4 signals were amplified using biotinyl-tyramide (TSA; Thermo Fisher Scientific) and Alexa 488–streptavidin (Invitrogen). Nuclei were visualized with Hoechst staining. Densitometric value corresponding to netrin-1 signal was quantified with AxioVision Release 4.6 software. Immunoblots were performed as already described using anti–phospho-DAPK and anti-DAPK (Sigma-Aldrich) (38), anti-DCC (1:500; Santa Cruz Biotechnology, Inc.), anti-neogenin (1:500; Santa Cruz Biotechnology, Inc.), anti-HA (1:7,500; Sigma-Aldrich), anti-HIS (1:1,000; QIAGEN), anti-MYCN (1:1000; BD), or anti-β-actin (1:1,000; Millipore) antibodies.

Netrin-1 ELISA assay. Detection of netrin-1 protein in IMR32 and CLB-Ge2 cell culture medium was performed using a modified ELISA assay. In brief, 96-well plates (Nunc-Immuno plate MaxiSorp; Thermo Fisher Scientific) were coated with 200 ng/well of purified recombinant extracellular domain of DCC (DCC-Ec-Fc). To minimize aspecific binding, each well was incubated with 100 µl of blocking solution, containing 5% (wt/vol) BSA (Sigma-Aldrich) in 0.05% PBS-Tween. 3 ml FBS free cell culture medium was added sequentially (300 µl/well) to coated 96-well plates and incubated for 1 h at 37°C. After three washes with 0.5% BSA/PBS, 100 µl of rat anti–netrin-1 antibody (diluted 1:500 in blocking solution) was added to each well and incubated for 30 min at 37°C. After extensive washing, each well was incubated with 100 µl HRP-conjugated goat anti–rat antibody (1:1,000; Jackson ImmunoResearch Laboratories) for 30 min at 37°C. After removal of unbound antibody by three washes in 0.5% BSA/PBS, the plates were incubated for 5 min at room temperature with ECL Western Blotting Substrate (Thermo Fisher Scientific). Luminescent signal was measured using a Luminoskan Ascent apparatus (Thermo Fisher Scientific).

Reporter assay. 10^5 cells were plated in 12-well plates and transfected with the firefly luciferase reporter under the control of the netrin-1 promoter (pGL3-NetP-Luc) or the pGL3 empty vector. All transfections were done in triplicate and the Dual-Luciferase Reporter Assay system (Promega) was performed 48 h after transfection according to the manufacturer's protocol, using the Luminoskan Ascent apparatus. As an internal control of transfection efficiency, the renilla luciferase-encoding plasmid (pRL-CMV; Promega) was cotransfected, and for each sample firefly luciferase activity was normalized to the renilla luciferase activity.

Chicken model for NB progression and dissemination. 10^7 NB cells suspended in 40 µl of complete medium were seeded on 10-d-old chick CAM. 10 µg DCC-5Fbn or the same PBS volume was injected in the tumor on days 11 and 14. For siRNA treatment, 4 µg of scramble or netrin-1 siRNA was injected under the same conditions as for DCC-5Fbn. On day 17, tumors were resected and the area was measured with AxioVision Release 4.6 software (Carl Zeiss, Inc.). To test the effect of DCC-5Fbn on metastasis regression, 3 µg DCC-5Fbn or PBS was injected on days 14 and 15 in a chorioallantoic vessel. To assess metastasis, lungs were harvested from the tumor-bearing embryos and genomic DNA was extracted with a NucleoSpin Tissue kit (Macherey-Nagel). Metastasis was quantified by PCR-based detection of the human Alu sequence using the primers 5′-ACGCCTGTAATCCCAGCACTT-3′ (sense) and 5′-TCGCCCAGGCTGGAGTGCA-3′ (antisense) with chick GAPDH-specific primers (sense, 5′-GAGGAAAGGTCGCCTGGTGGATCG-3′; antisense, 5′-GGTGAGGACAAGCAGTGAGGAACG-3′) as controls. For both couples of primers, metastasis was assessed by polymerase activation at 95°C for 2 min followed by 30 cycles at 95°C for 30 s, 63°C for 30 s, and 72°C for 30 s. Genomic DNA extracted from lungs of healthy chick embryos was used to determine the threshold between NB cell–invaded and –noninvaded lungs. To monitor apoptosis in primary tumors, primary tumors and surrounding CAM were resected and broken up in lysis buffer and caspase-3 activity was measured using the Caspase 3/CPP32 Fluorimetric Assay kit.

NB metastasis in *nude* mice. 7-wk-old (20–22 g body weight) female athymic nu/nu mice were obtained from Charles River Laboratories. The mice were housed in sterilized filter-topped cages and maintained in a pathogen-free animal facility. IGR-N-91–derived PTX and Myoc cell lines were implanted by i.v. injection of 10^6 cells in 130 µl of PBS into a tail vein (day 0). 20 µg DCC-5Fbn or PBS with equal volume was i.p. injected daily during 22 d. Lungs were harvested on day 23. Lung genomic DNA was extracted with the NucleoSpin Tissue kit, and quantification of human tumor cells in lungs was done by PCR-based detection of the human Alu sequence using the primers 5′-CACCTGTAATCCCAGCACTTT-3′ (sense) and 5′-CCCAGGCTGGAGTGCAGT-3′ (antisense), using 25 ng of genomic DNA as previously described (56). PCR was performed under the following conditions: 95°C for 2 min, 30 cycles at 95°C for 30 s, 65°C for 20 s, and 72°C for 20 s. Quantification of human DNA in mice lungs was based on a standard curve using human genomic DNA isolated from PTX and Myoc cell lines.

Online supplemental material. Fig. S1 associates netrin-1 and DCC expression in NB tumors with their apoptosis and invasion molecular signatures obtained with microarrays. Fig. S2 presents netrin-1 mRNA and protein expression in NB cell lines and shows CLB-VolMo netrin-1–high cell line sensitivity to DCC-5Fbn decoy fragment. In Fig. S3, MYCN and neogenin implication in netrin-1 siRNA-induced cell death is studied, and specificity and efficiency of UNC5H siRNAs are presented at the mRNA, protein, and cellular levels. Online supplemental material is available at http://www.jem.org/cgi/content/full/jem.20082299/DC1.

We thank M.M. Coissieux, C. Guix, M.L. Puiffe, I. Iacono, and S. Bréjon for technical assistance. We thank J. Bouzas, J.G. Delcros, and P. Leissner for excellent support. We thank Dale E. Bredesen for precious advice and text correction.

This work was supported by the Ligue Contre le Cancer (P. Mehlen), the Agence Nationale de la Recherche (P. Mehlen), the Institut National du Cancer (J. Bénard, A. Puisieux, and P. Mehlen), the Société Francaise des Cancers de l'Enfant (J. Bénard), The French Health Minister (J. Bénard and D. Valteau-Couanet), The EU fundings Hermione (P. Mehlen) and APOSYS (P. Mehlen), the Centre National de la Recherche Scientifique, and the Centre Léon Bérard.

The authors have no conflicting financial interests.

Submitted: 14 October 2008
Accepted: 3 March 2009

REFERENCES

1. Mehlen, P., S. Rabizadeh, S.J. Snipas, N. Assa-Munt, G.S. Salvesen, and D.E. Bredesen. 1998. The DCC gene product induces apoptosis by a mechanism requiring receptor proteolysis. *Nature.* 395:801–804.
2. Llambi, F., F. Causeret, E. Bloch-Gallego, and P. Mehlen. 2001. Netrin-1 acts as a survival factor via its receptors UNC5H and DCC. *EMBO J.* 20:2715–2722.
3. Thibert, C., M.A. Teillet, F. Lapointe, L. Mazelin, N.M. Le Douarin, and P. Mehlen. 2003. Inhibition of neuroepithelial patched-induced apoptosis by sonic hedgehog. *Science.* 301:843–846.
4. Stupack, D.G., X.S. Puente, S. Boutsaboualoy, C.M. Storgard, and D.A. Cheresh. 2001. Apoptosis of adherent cells by recruitment of caspase-8 to unligated integrins. *J. Cell Biol.* 155:459–470.
5. Matsunaga, E., S. Tauszig-Delamasure, P.P. Monnier, B.K. Mueller, S.M. Strittmatter, P. Mehlen, and A. Chedotal. 2004. RGM and its receptor neogenin regulate neuronal survival. *Nat. Cell Biol.* 6:749–755.
6. Rabizadeh, S., J. Oh, L.T. Zhong, J. Yang, C.M. Bitler, L.L. Butcher, and D.E. Bredesen. 1993. Induction of apoptosis by the low-affinity NGF receptor. *Science.* 261:345–348.
7. Bordeaux, M.C., C. Forcet, L. Granger, V. Corset, C. Bidaud, M. Billaud, D.E. Bredesen, P. Edery, and P. Mehlen. 2000. The RET

proto-oncogene induces apoptosis: a novel mechanism for Hirschsprung disease. *EMBO J.* 19:4056–4063.
8. Mourali, J., A. Benard, F.C. Lourenco, C. Monnet, C. Greenland, C. Moog-Lutz, C. Racaud-Sultan, D. Gonzalez-Dunia, M. Vigny, P. Mehlen, et al. 2006. Anaplastic lymphoma kinase is a dependence receptor whose proapoptotic functions are activated by caspase cleavage. *Mol. Cell. Biol.* 26:6209–6222.
9. Tauszig-Delamasure, S., L.Y. Yu, J.R. Cabrera, J. Bouzas-Rodriguez, C. Mermet-Bouvier, C. Guix, M.C. Bordeaux, U. Arumae, and P. Mehlen. 2007. The TrkC receptor induces apoptosis when the dependence receptor notion meets the neurotrophin paradigm. *Proc. Natl. Acad. Sci. USA.* 104:13361–13366.
10. Del Rio, G., D.J. Kane, K.D. Ball, and D.E. Bredesen. 2007. A novel motif identified in dependence receptors. *PLoS One.* 2:e463.
11. Mehlen, P., and C. Thibert. 2004. Dependence receptors: between life and death. *Cell. Mol. Life Sci.* 61:1854–1866.
12. Bredesen, D.E., P. Mehlen, and S. Rabizadeh. 2005. Receptors that mediate cellular dependence. *Cell Death Differ.* 12:1031–1043.
13. Serafini, T., S.A. Colamarino, E.D. Leonardo, H. Wang, R. Beddington, W.C. Skarnes, and M. Tessier-Lavigne. 1996. Netrin-1 is required for commissural axon guidance in the developing vertebrate nervous system. *Cell.* 87:1001–1014.
14. Keino-Masu, K., M. Masu, L. Hinck, E.D. Leonardo, S.S. Chan, J.G. Culotti, and M. Tessier-Lavigne. 1996. Deleted in colorectal cancer (DCC) encodes a netrin receptor. *Cell.* 87:175–185.
15. Forcet, C., E. Stein, L. Pays, V. Corset, F. Llambi, M. Tessier-Lavigne, and P. Mehlen. 2002. Netrin-1-mediated axon outgrowth requires deleted in colorectal cancer-dependent MAPK activation. *Nature.* 417:443–447.
16. Ackerman, S.L., L.P. Kozak, S.A. Przyborski, L.A. Rund, B.B. Boyer, and B.B. Knowles. 1997. The mouse rostral cerebellar malformation gene encodes an UNC-5-like protein. *Nature.* 386:838–842.
17. Hong, K., L. Hinck, M. Nishiyama, M.M. Poo, M. Tessier-Lavigne, and E. Stein. 1999. A ligand-gated association between cytoplasmic domains of UNC5 and DCC family receptors converts netrin-induced growth cone attraction to repulsion. *Cell.* 97:927–941.
18. Mehlen, P., and A. Puisieux. 2006. Metastasis: a question of life or death. *Nat. Rev. Cancer.* 6:449–458.
19. Grady, W.M. 2007. Making the case for DCC and UNC5C as tumor-suppressor genes in the colon. *Gastroenterology.* 133:2045–2049.
20. Mazelin, L., A. Bernet, C. Bonod-Bidaud, L. Pays, S. Arnaud, C. Gespach, D.E. Bredesen, J.Y. Scoazec, and P. Mehlen. 2004. Netrin-1 controls colorectal tumorigenesis by regulating apoptosis. *Nature.* 431:80–84.
21. Bernet, A., L. Mazelin, M.M. Coissieux, N. Gadot, S.L. Ackerman, J.Y. Scoazec, and P. Mehlen. 2007. Inactivation of the UNC5C Netrin-1 receptor is associated with tumor progression in colorectal malignancies. *Gastroenterology.* 133:1840–1848.
22. Fearon, E.R., K.R. Cho, J.M. Nigro, S.E. Kern, J.W. Simons, J.M. Ruppert, S.R. Hamilton, A.C. Preisinger, G. Thomas, K.W. Kinzler, et al. 1990. Identification of a chromosome 18q gene that is altered in colorectal cancers. *Science.* 247:49–56.
23. Kinzler, K.W., and B. Vogelstein. 1996. Lessons from hereditary colorectal cancer. *Cell.* 87:159–170.
24. Thiebault, K., L. Mazelin, L. Pays, F. Llambi, M.O. Joly, J.C. Saurin, J.Y. Scoazec, G. Romeo, and P. Mehlen. 2003. The netrin-1 receptors UNC5H are putative tumor suppressors controlling cell death commitment. *Proc. Natl. Acad. Sci. USA.* 100:4173–4178.
25. Shin, S.K., T. Nagasaka, B.H. Jung, N. Matsubara, W.H. Kim, J.M. Carethers, C.R. Boland, and A. Goel. 2007. Epigenetic and genetic alterations in Netrin-1 receptors UNC5C and DCC in human colon cancer. *Gastroenterology.* 133:1849–1857.
26. Evans, A.E., G.J. D'Angio, and J. Randolph. 1971. A proposed staging for children with neuroblastoma. Children's cancer study group A. *Cancer.* 27:374–378.
27. Matthay, K.K., J.G. Villablanca, R.C. Seeger, D.O. Stram, R.E. Harris, N.K. Ramsay, P. Swift, H. Shimada, C.T. Black, G.M. Brodeur, et al. 1999. Treatment of high-risk neuroblastoma with intensive chemotherapy, radiotherapy, autologous bone marrow transplantation, and 13-cis-retinoic acid. Children's Cancer Group. *N. Engl. J. Med.* 341:1165–1173.
28. Valteau-Couanet, D., J. Michon, A. Boneu, C. Rodary, Y. Perel, C. Bergeron, H. Rubie, C. Coze, D. Plantaz, F. Bernard, et al. 2005. Results of induction chemotherapy in children older than 1 year with a stage 4 neuroblastoma treated with the NB 97 French Society of Pediatric Oncology (SFOP) protocol. *J. Clin. Oncol.* 23:532–540.
29. Reale, M.A., M. Reyes-Mugica, W.E. Pierceall, M.C. Rubinstein, L. Hedrick, S.L. Cohn, A. Nakagawara, G.M. Brodeur, and E.R. Fearon. 1996. Loss of DCC expression in neuroblastoma is associated with disease dissemination. *Clin. Cancer Res.* 2:1097–1102.
30. Krause, A., V. Combaret, I. Iacono, B. Lacroix, C. Compagnon, C. Bergeron, S. Valsesia-Wittmann, P. Leissner, B. Mougin, and A. Puisieux. 2005. Genome-wide analysis of gene expression in neuroblastomas detected by mass screening. *Cancer Lett.* 225:111–120.
31. Furne, C., N. Rama, V. Corset, A. Chedotal, and P. Mehlen. 2008. Netrin-1 is a survival factor during commissural neuron navigation. *Proc. Natl. Acad. Sci. USA.* 105:14465–14470.
32. Paradisi, A., C. Maisse, A. Bernet, M. Coissieux, M. Maccarrone, J. Scoazec, and P. Mehlen. 2008. NF-κB regulates netrin-1 expression and affects the conditional tumor suppressive activity of the netrin-1 receptors. *Gastroenterology.* 135:1248–1257.
33. Fitamant, J., C. Guenebeaud, M.M. Coissieux, C. Guix, I. Treilleux, J.Y. Scoazec, T. Bachelot, A. Bernet, and P. Mehlen. 2008. Netrin-1 expression confers a selective advantage for tumor cell survival in metastatic breast cancer. *Proc. Natl. Acad. Sci. USA.* 105:4850–4855.
34. Reale, M.A., G. Hu, A.I. Zafar, R.H. Getzenberg, S.M. Levine, and E.R. Fearon. 1994. Expression and alternative splicing of the deleted in colorectal cancer (DCC) gene in normal and malignant tissues. *Cancer Res.* 54:4493–4501.
35. Meyerhardt, J.A., A.T. Look, S.H. Bigner, and E.R. Fearon. 1997. Identification and characterization of neogenin, a DCC-related gene. *Oncogene.* 14:1129–1136.
36. Cole, S.J., D. Bradford, and H.M. Cooper. 2007. Neogenin: a multifunctional receptor regulating diverse developmental processes. *Int. J. Biochem. Cell Biol.* 39:1569–1575.
37. Rajagopalan, S., L. Deitinghoff, D. Davis, S. Conrad, T. Skutella, A. Chedotal, B.K. Mueller, and S.M. Strittmatter. 2004. Neogenin mediates the action of repulsive guidance molecule. *Nat. Cell Biol.* 6:756–762.
38. Llambi, F., F.C. Lourenco, D. Gozuacik, C. Guix, L. Pays, G. Del Rio, A. Kimchi, and P. Mehlen. 2005. The dependence receptor UNC5H2 mediates apoptosis through DAP-kinase. *EMBO J.* 24:1192–1201.
39. Ferrandis, E., J. Da Silva, G. Riou, and J. Benard. 1994. Coactivation of the MDR1 and MYCN genes in human neuroblastoma cells during the metastatic process in the nude mouse. *Cancer Res.* 54:2256–2261.
40. Link, B.C., U. Reichelt, M. Schreiber, J.T. Kaiti, R. Wachowiak, D. Bogoevski, M. Bubenheim, G. Cataldegirmen, K.A. Gawad, R. Issa, et al. 2007. Prognostic implications of Netrin-1 expression and its receptors in patients with adenocarcinoma of the pancreas. *Ann. Surg. Oncol.* 14:2591–2599.
41. Inbal, B., O. Cohen, S. Polak-Charcon, J. Kopolovic, E. Vadai, L. Eisenbach, and A. Kimchi. 1997. DAP kinase links the control of apoptosis to metastasis. *Nature.* 390:180–184.
42. Stupack, D.G., T. Teitz, M.D. Potter, D. Mikolon, P.J. Houghton, V.J. Kidd, J.M. Lahti, and D.A. Cheresh. 2006. Potentiation of neuroblastoma metastasis by loss of caspase-8. *Nature.* 439:95–99.
43. Yebra, M., A.M. Montgomery, G.R. Diaferia, T. Kaido, S. Silletti, B. Perez, M.L. Just, S. Hildbrand, R. Hurford, E. Florkiewicz, et al. 2003. Recognition of the neural chemoattractant Netrin-1 by integrins alpha6beta4 and alpha3beta1 regulates epithelial cell adhesion and migration. *Dev. Cell.* 5:695–707.
44. Park, K.W., D. Crouse, M. Lee, S.K. Karnik, L.K. Sorensen, K.J. Murphy, C.J. Kuo, and D.Y. Li. 2004. The axonal attractant Netrin-1 is an angiogenic factor. *Proc. Natl. Acad. Sci. USA.* 101:16210–16215.
45. Lu, X., F. Le Noble, L. Yuan, Q. Jiang, B. De Lafarge, D. Sugiyama, C. Breant, F. Claes, F. De Smet, J.L. Thomas, et al. 2004. The netrin receptor UNC5B mediates guidance events controlling morphogenesis of the vascular system. *Nature.* 432:179–186.
46. Nguyen, A., and H. Cai. 2006. Netrin-1 induces angiogenesis via a DCC-dependent ERK1/2-eNOS feed-forward mechanism. *Proc. Natl. Acad. Sci. USA.* 103:6530–6535.

47. Wilson, B.D., M. Ii, K.W. Park, A. Suli, L.K. Sorensen, F. Larrieu-Lahargue, L.D. Urness, W. Suh, J. Asai, G.A. Kock, et al. 2006. Netrins promote developmental and therapeutic angiogenesis. *Science*. 313:640–644.
48. Jiang, Y., L. Min-tsai, and M.D. Gershon. 2003. Netrins and DCC in the guidance of migrating neural Crest-derived cells in the developing bowel and pancreas. *Dev. Biol.* 258:364–384.
49. Roperch, J.P., K. El Ouadrani, A. Hendrix, S. Emami, O. De Wever, G. Melino, and C. Gespach. 2008. Netrin-1 induces apoptosis in human cervical tumor cells via the TAp73alpha tumor suppressor. *Cancer Res.* 68:8231–8239.
50. Bourhis, J., C. Dominici, H. McDowell, G. Raschella, G. Wilson, M.A. Castello, E. Plouvier, J. Lemerle, G. Riou, J. Benard, et al. 1991. N-myc genomic content and DNA ploidy in stage IVS neuroblastoma. *J. Clin. Oncol.* 9:1371–1375.
51. Rubie, H., D. Plantaz, C. Coze, J. Michon, D. Frappaz, M.C. Baranzelli, P. Chastagner, M.C. Peyroulet, and O. Hartmann. 2001. Localised and unresectable neuroblastoma in infants: excellent outcome with primary chemotherapy. Neuroblastoma Study Group, Societe Francaise d'Oncologie Pediatrique. *Med. Pediatr. Oncol.* 36:247–250.
52. Ambros, I.M., J. Benard, M. Boavida, N. Bown, H. Caron, V. Combaret, J. Couturier, C. Darnfors, O. Delattre, J. Freeman-Edward, et al. 2003. Quality assessment of genetic markers used for therapy stratification. *J. Clin. Oncol.* 21:2077–2084.
53. Ghoumari, A.M., R. Wehrle, O. Bernard, C. Sotelo, and I. Dusart. 2000. Implication of Bcl-2 and Caspase-3 in age-related Purkinje cell death in murine organotypic culture: an in vitro model to study apoptosis. *Eur. J. Neurosci.* 12:2935–2949.
54. Vandesompele, J., K. De Preter, F. Pattyn, B. Poppe, N. Van Roy, A. De Paepe, and F. Speleman. 2002. Accurate normalization of real-time quantitative RT-PCR data by geometric averaging of multiple internal control genes. *Genome Biol.* 3:research0034.1–0034.11.
55. Gotoh, T., H. Hosoi, T. Iehara, Y. Kuwahara, S. Osone, K. Tsuchiya, M. Ohira, A. Nakagawara, H. Kuroda, and T. Sugimoto. 2005. Prediction of MYCN amplification in neuroblastoma using serum DNA and real-time quantitative polymerase chain reaction. *J. Clin. Oncol.* 23:5205–5210.
56. Schneider, T., F. Osl, T. Friess, H. Stockinger, and W. Scheuer. 2002. Quantification of human Alu sequences by real-time PCR–an improved method to measure therapeutic efficacy of anti-metastatic drugs in human xenotransplants. *Clin. Exp. Metastasis.* 19:571–582.

Oncogene (2009) 28, 3631–3641
© 2009 Macmillan Publishers Limited All rights reserved 0950-9232/09 $32.00
www.nature.com/onc

ORIGINAL ARTICLE

Plk1 regulates liver tumor cell death by phosphorylation of TAp63

S Komatsu[1,2], H Takenobu[1], T Ozaki[1], K Ando[1], N Koida[1], Y Suenaga[1], T Ichikawa[1], T Hishiki[2], T Chiba[3], A Iwama[3], H Yoshida[2], N Ohnuma[2], A Nakagawara[1] and T Kamijo[1]

[1]*Division of Biochemistry, Chiba Cancer Center Research Institute, Chiba, Japan;* [2]*Department of Pediatric Surgery, Graduate School of Medicine, Chiba University, Chiba, Japan and* [3]*Department of Cellular and Molecular Medicine, Graduate School of Medicine, Chiba University, Chiba, Japan*

We previously found that Plk1 inhibited the p53/p73 activity through its direct phosphorylation. In this study, we investigated the functional role of Plk1 in modulating the p53 family member TAp63, resulting in the control of apoptotic cell death in liver tumor cells. Immunoprecipitation and *in vitro* pull-down assay showed that p63 binds to the kinase domain of Plk1 through its DNA-binding region. *in vitro* kinase assay indicated that p63 is phosphorylated by Plk1 at Ser-52 of the transactivating (TA) domain. Plk1 decreased the protein stability of TAp63 by its phosphorylation and suppressed TAp63-induced cell death. Furthermore, Plk1 knockdown in *p53*-mutated liver tumor cells transactivated p53 family downstream effectors, *PUMA*, *p21*$^{Cip1/WAF1}$ and *14-3-3σ*, and induced apoptotic cell death. Double knockdown of Plk1/p63 attenuated Plk1 knockdown-induced apoptotic cell death and transactivation. Intriguingly, both Plk1 and p63 are highly expressed in the side population (SP) fraction of liver tumor cells compared to non-SP fraction cells, suggesting the significance of Plk1/TAp63 in the control of cell death in tumor-initiating SP fraction cells. Thus, Plk1 controls TAp63 by its phosphorylation and regulates apoptotic cell death in liver tumor cells. Plk1/TAp63 may be a suitable candidate as a molecular target of liver tumor treatments.
Oncogene (2009) **28,** 3631–3641; doi:10.1038/onc.2009.216; published online 10 August 2009

Keywords: p63; phosphorylation; Plk1; apoptosis

Introduction

Polo-like kinase 1 (Plk1) is a key regulator of progression through mitosis. Although Plk1 seems to be dispensable for entry into mitosis, its role in spindle formation and exit from mitosis is crucial (Eckerdt and Strebhardt, 2006). Plk1 is overexpressed in human tumors and has prognostic potential in cancer (Strebhardt and Ullrich, 2006). Previously, our laboratory reported that Plk1 is highly expressed in hepatoblastoma samples and patients with a high expression of Plk1 showed significantly poorer prognosis than those with a low expression (Yamada *et al.*, 2004), indicating Plk1's involvement in carcinogenesis and its potential as a therapeutic target in liver cell malignancy. In fact, depletion of Plk1 by small interfering RNA (siRNA) treatment resulted in the arrest of cell-cycle progression at the G2/M phase, such that proliferation was dramatically reduced and apoptosis increased in multiple cancer cell lines (Strebhardt and Ullrich, 2006); however, the downstream effectors and the molecular mechanism of Plk1-depletion-induced apoptosis have not been identified in detail. In the previous paper, we found that Plk1 inhibits the pro-apoptotic function of p53 through physical interaction (Ando *et al.*, 2004) and that Plk1 has the ability to bind to and phosphorylate transactivating (TA)p73 at Thr27, thereby inhibiting its transcriptional as well as pro-apoptotic activity (Koida *et al.*, 2008), suggesting that p53 family molecules have a significant function in Plk1-depletion-induced apoptosis in cancer cells.

The p63 gene has strong homology to the tumor suppressor p53 and the related gene, p73. p63 is actually the oldest evolutionary conserved member of the p53 family phylogenetically (Blandino and Dobbelstein, 2004). It is a tumor suppressor gene and the most frequent site of genetic alterations in human cancers (Vousden and Lu, 2002). p53 protein is a transcription factor that regulates the expression of a wide variety of genes involved in cell-cycle arrest and apoptosis in response to genotoxic or cellular stress (Levine, 1997; Yang *et al.*, 1998). Post-translational modification of p53 families is a key to their regulation. By contrast, reports on p63 phosphorylation are limited and its analysis remains to be confirmed (Westfall *et al.*, 2005; Suh *et al.*, 2006; MacPartlin *et al.*, 2008). In general, many functional parallels are found among p53, TAp73 and TAp63. When ectopically overexpressed in cell culture, TAp63 and TAp73 closely mimic the transcriptional activity and the biological function of p53. In reporter assays, p63/73-responsive promoters include well-known p53 target genes involved in anti-proliferative and pro-apoptotic cellular stress responses such as *p21*$^{Cip1/WAF1}$, *14-3-3σ*, *Bax*, and so on (Candi *et al.*, 2007). Furthermore, both p63 and p73 isoforms contribute to the regulation of cell survival and apoptosis in human

Correspondence: Dr T Kamijo, Division of Biochemistry, Chiba Cancer Center Research Institute, 666-2 Nitona, Chuo-ku, Chiba, Chiba 260-8717, Japan.
E-mail: tkamijo@chiba-cc.jp
Received 27 November 2008; revised 17 June 2009; accepted 23 June 2009; published online 10 August 2009

tumors (Moll and Slade, 2004). Indeed, their ability to regulate apoptosis is clearly a major mechanism by which these genes contribute to human tumorigenesis (Rocco *et al.*, 2006). Initial studies in mice have shown the pro-apoptotic activity of endogenous p63 and p73. Germline deletion of p63 or p73 yielded mouse embryo fibroblasts (MEFs) that were less sensitive to DNA-damage-induced apoptosis than to wild-type cells when transformed by adenoviral E1A protein (Flores *et al.*, 2002). Although the above-mentioned lines of evidence indicate that p63 has an important function in DNA damage, controlling cell-cycle arrest and apoptosis, and in human cancer, its precise role in tumorigenesis remains to be elucidated. For example, unlike p53, p63 is rarely mutated in human cancers (Kato *et al.*, 1999), thus indicating it is not a canonical tumor suppressor. Furthermore, a potential role for p63 in carcinogenesis is supported by the finding of p63 genomic locus amplification and/or overexpression in more than 80% of primary head and neck squamous cell carcinoma as well as in other squamous epithelial cell malignancies (Massion *et al.*, 2003). On the other hand, some tumor types have been reported to lose p63 expression, suggesting the acceleration of tumorigenesis by p63 downregulation (Urist *et al.*, 2002; Koga *et al.*, 2003).

In liver cell malignancy, the precise role of p63 in tumorigenesis and its clinical significance have not been elucidated. Liver cancer ranks fifth in the world among human cancers for incidence and third for mortality (Parkin *et al.*, 2001). Hepatocellular carcinoma (HCC), the most common malignant tumor of the liver, has an extremely unfavorable prognosis (over 95% mortality after 5 years), because of, in particular, the resistance of HCC cells to chemotherapy or radiotherapy (Bruix and Llovet, 2002). A high incidence of p53 mutation is observed in developing countries (53%; Shen and Ong, 2004), although p53 missense mutations are observed in ~25% of HCC samples from industrialized countries, where the tumor essentially develops from alcohol-generated cirrhosis (Montesano *et al.*, 1997). Previous reports indicated that the expression of TAp63 and deltaNp63 in HCC cell lines and the upregulation of TAp63 in response to certain forms of DNA damage accompanied with the increase in p53 target gene transcription (Petitjean *et al.*, 2005) and treatment of HCC with chemotherapeutic drugs resulted in a dramatic increase in TAp63alpha levels (Gressner *et al.*, 2005).

In this study, we have found that Plk1 directly binds to TAp63alpha and phosphorylates TAp63 at the Ser-52, resulting in inhibition of its transcriptional activities caused by acceleration of protein degradation. To the best of our knowledge, this is the first report to determine the phosphorylated serine residue in the TA domain of p63. Plk1-depletion-induced apoptosis and activated p53 pathway downstream effectors are partially cancelled by p63 depletion in HCC cells. Furthermore, our finding suggests the possibility that Plk1/p63 appears to be an important candidate for cancer stem-cell-targeted therapy in liver cell malignancy.

Results

Physical and functional interaction between Plk1 and p63

First, we examined whether Plk1 interacts with TAp63. COS-7 cells were transiently transfected with the expression plasmid for FLAG-tagged Plk1 and/or HA-tagged TAp63alpha. Whole-cell lysates prepared from transfected cells were immunoprecipitated with a monoclonal anti-HA antibody, and the immunoprecipitates were analysed by immunoblotting with a monoclonal anti-FLAG antibody. As shown in Figure 1a, FLAG-Plk1 was co-immunoprecipitated with HA-TAp63, and the analysis of the anti-FLAG immunoprecipitates also showed that HA-TAp63 is co-immunoprecipitated with FLAG-Plk1.

Furthermore, endogenous interaction between Plk1 and p63 was also detected using HaCaT cells (Figure 1b). These results indicate that Plk1 interacts with p63 in mammalian cultured cells. As HaCaT cells show a high expression level of deltaNp63, this

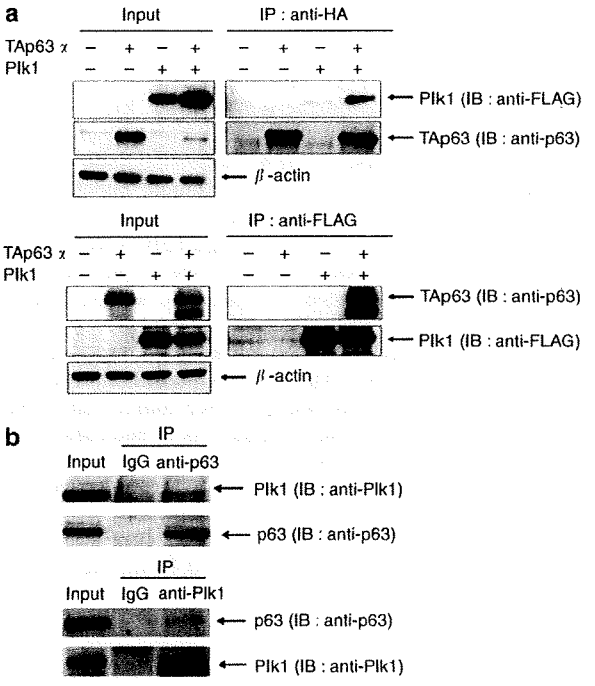

Figure 1 Interaction between Plk1 and p63 in cells. (**a**) Interaction between exogenously expressed Plk1 and TAp63. Whole-cell lysates from COS-7 cells transfected with FLAG-Plk1 and/or HA-TAp63 expression plasmids were immunoprecipitated with monoclonal anti-HA antibody (clone 3F10, Roche) and monoclonal anti-FLAG antibody (clone M2, Sigma), and immunoblotted with monoclonal anti-FLAG antibody and monoclonal anti-p63 antibody (clone 4a4) as indicated, to observe the interaction. Control immunoprecipitation experiments and loading control β-actin signals were also indicated. (**b**) Interaction between endogenous Plk1 and p63. A total of 500 μg of nuclear extract from HaCaT cells were immunoprecipitated with IgG, monoclonal anti-63 antibody (clone 4A4) or monoclonal anti-Plk1 antibody and subjected to SDS–PAGE (polyacrylamide gel electrophoresis) and protein transfer. The transferred membranes were immunoblotted with monoclonal anti-Plk1 antibody or monoclonal anti-p63 (clone 4a4) antibody to observe the interaction. *IgG*, mouse IgG.

interaction was supposed to be between Plk1 and deltaNp63.

TAp63 binds to the kinase domain of Plk1 through its DNA-binding region

Next, to map the p63-interacting domain on Plk1, we constructed FLAG-tagged Plk1 deletion mutants, including Plk1-(1–401), Plk1-(1–329) and Plk1-(1–98) (Figure 2a). We then tested the interaction between TAp63alpha and each of these Plk1 deletion mutants. COS-7 cells were transfected with the expression plasmid encoding TAp63alpha and each Plk1 deletion mutant, and co-immunoprecipitation experiments were carried out to determine the interaction.

We found that Plk1-(1–401) and Plk1-(1–329) retained the ability to bind to TAp63alpha, whereas Plk1-(1–98) did not (Figure 2b). These results indicate that Plk1 physically interacts with TAp63alpha through its 99–329 amino acid residues. To identify the essential region of TAp63alpha required for the interaction with Plk1, we carried out *in vitro* pull-down assays. The indicated glutathione-*S*-transferase (GST)–TAp63alpha deletion mutants (Figure 2c) were purified with glutathione-sepharose beads. Each of these GST fusion proteins was incubated with radiolabeled FLAG-Plk1, which was generated by the *in vitro* transcription/translation system in the presence of [^{35}S]methionine. As clearly shown in Figure 2d, radiolabeled FLAG-Plk1 was efficiently pulled down by GST–TAp63alpha-(282–357), implying that the region between amino acid residues 282 and 353 of TAp63alpha is important for the interaction with Plk1. As this binding site is common between TAp63 and deltaNp63, in Figure 1b, it is believed that Plk1 binds to TAp63 as well as to deltaNp63.

Plk1 directly phosphorylates Ser-52 of TAp63

Furthermore, to address whether Plk1 could phosphorylate TAp63, we carried out an *in vitro* kinase reaction. GST and GST–TAp63alpha fusion proteins were incubated with the active form of Plk1 in the presence of [γ^{32}P]ATP. The reaction mixtures were separated by SDS–polyacrylamide gel electrophoresis (PAGE) and subjected to autoradiography (Figure 3a). The results suggested that Plk1 phosphorylates the region between amino acid residues 20 and 96 of TAp63.

As described earlier (Nakajima *et al*., 2003), a sequence (D/E)*X*(S/T)ΦD/E) (where *X* is any amino acid and Φ a hydrophobic amino acid) was identified as a consensus motif for Plk1-dependent phosphorylation. According to the search for a putative phosphorylation site targeted by Plk1 within the amino acid sequence of TAp63 (residues 20–96), we identified related motifs, (39EPSEDG44 and 50EISMDC55), in the NH2-terminal portion of TAp63alpha (Figure 3b).

To further confirm whether Ser-41 or Ser-52 of TAp63 could be phosphorylated by Plk1, we generated a mutant form of GST-p63-(1–102), termed as 'S41A' and 'S52A,' where Ser-41 or Ser-52 was substituted to Ala. Purified GST fusion proteins were subjected to the *in vitro* kinase reaction. As shown in Figure 3c, GST–TAp63-(1–102) and S41A mutant were strongly radiolabeled in the presence of Plk1, whereas S52A mutant was not labeled, indicating that Ser-52 of TAp63 is at least one of the phosphorylation sites targeted by Plk1, and is located in the transcriptional domain of TAp63. In addition, it seemed to be interesting that the molecular size of the mutant p63(1–102)S52A was smaller than that of p63 (1–102)S41A and p63(1–102), suggesting the effect of phosphorylation of S52 of TAp63 on the molecular weight of the 1–102 peptide.

Plk1 represses TAp63-mediated transcriptional activation

To address the effect of Plk1 on the transcriptional activity of TAp63, we carried out luciferase reporter assays. H1299 cells were co-transfected with a constant amount of the expression plasmid for TAp63alpha, the luciferase reporter construct carrying p53/p63-responsive *p21$^{Cip1/WAF1}$*, *BAX* or *MDM2* promoter and *Renilla* luciferase cDNA (pRL-TK) together with or without increasing amounts of FLAG-Plk1 expression plasmid. Enforced expression of FLAG-Plk1 significantly reduced luciferase activities driven by the indicated promoters in a dose-dependent manner (Figure 4a). These results suggest that Plk1 has the ability to repress the transcriptional activity of TAp63. Furthermore, to examine whether the kinase activity of Plk1 could be necessary for the inhibition of TAp63 function, we tested the possible effect of the kinase-deficient mutant form of Plk1, Plk1(K82M) (Supplementary data) on TAp63. For this purpose, we first examined whether Plk1(K82M) could interact with TAp63 in cells. The interaction between TAp63alpha and Plk1(K82M) was confirmed bi-directionally (Figure 4b). These results suggest that the kinase-deficient mutant form of Plk1 retains the ability to interact with TAp63 in cells. To further examine the effect of the kinase activity of Plk1 on TAp63 function, we carried out luciferase reporter assays. H1299 cells were co-transfected with a constant amount of the expression plasmid for TAp63alpha, a luciferase reporter construct bearing p53/p63-responsive *p21$^{Cip1/WAF1}$*, *BAX* or *MDM2* promoter and *Renilla* luciferase cDNA together with or without increasing amounts of FLAG-Plk1(K82M). As shown in Figure 4c, FLAG-Plk1(K82M) had a negligible effect on the transcriptional activity of TAp63. Collectively, these results indicate that kinase activity of Plk1 is required for the inhibition of TAp63 function.

Plk1 reduces the protein stability of TAp63 by its phosphorylation and suppresses TAp63-induced cell death

Next, we checked the effect of Plk1 on TAp63-induced cell death. H1299 cells were transfected with mock, TAp63alpha, TAp63alpha/Plk1 or TAp63alpha/KD Plk1, and at 24 h after transfection, the cells were observed. TAp63alpha-transfected cells showed the inhibition of cell growth and increase in shrunken and floating cells compared with mock transfection;

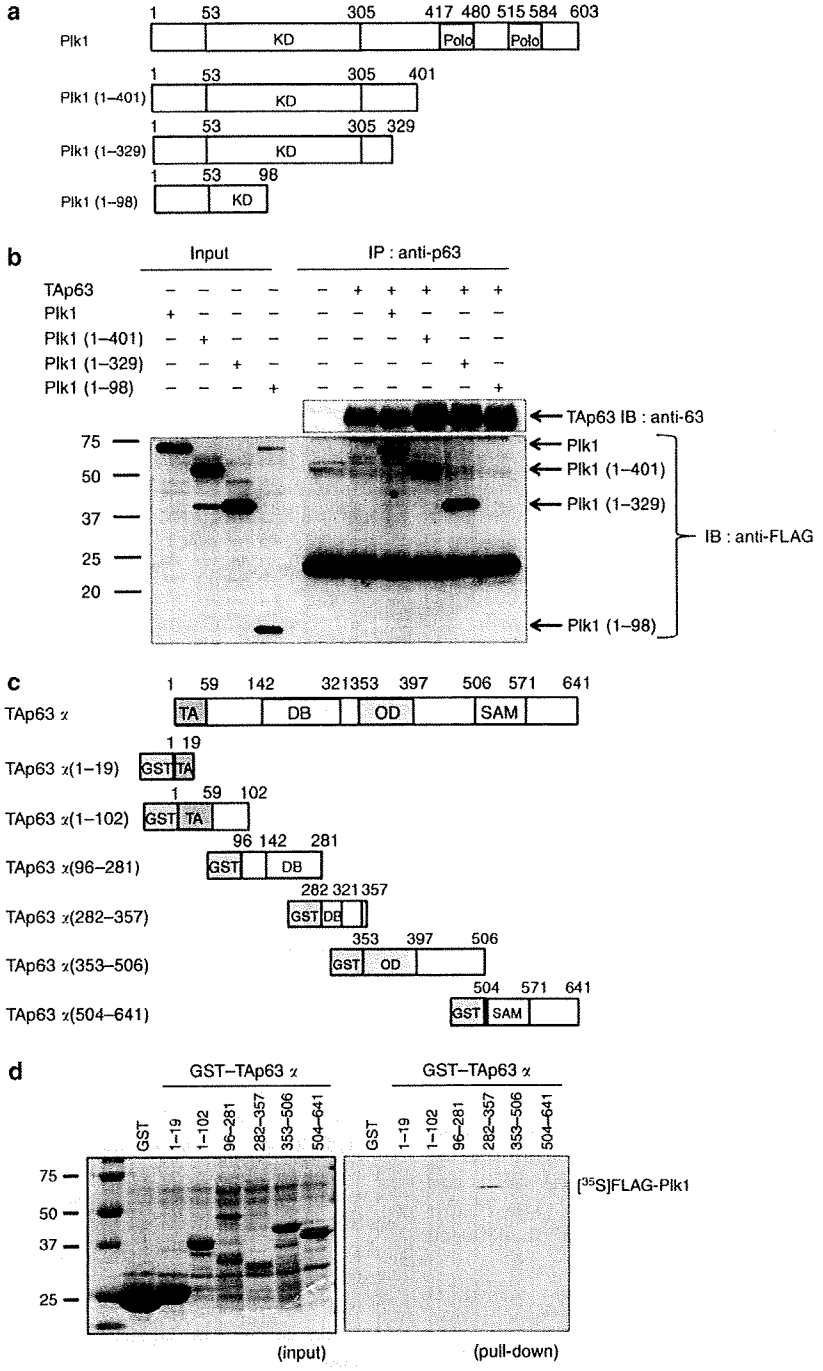

Figure 2 TAp63 binds to the kinase domain of Plk1 through its DNA-binding region. (**a**) Schematic representation of Plk1 deletion mutants. *KD*, kinase domain; *Polo*, polo-box; numbers indicate amino acid position. (**b**) Interaction between Plk1 deletion mutants and TAp63. Whole-cell lysates from COS-7 cells transfected with the indicated expression plasmids were immunoprecipitated with monoclonal anti-p63 antibody and immunoblotted with monoclonal anti-FLAG antibody to observe the interaction between Plk1 deletion mutants and TAp63. Immunoprecipitation with mouse IgG was used as a negative control. Equal amounts of protein derived from cell lysates were immunoblotted with monoclonal anti-FLAG antibody. Control immunoprecipitation–immunoblotting experiments of TAp63 were also indicated. (**c**) Domain structure of wild-type TAp63alpha and a schematic representation of GST-tagged TAp63alpha deletion mutants. *TA*, transactivation domain; *DB*, DNA-binding domain; *OD*, oligomerization domain; *SAM*, sterileá-motif domain. Numbers indicate amino acid positions. (**d**) *In vitro* pull-down assay. An equal amount of radiolabeled FLAG-Plk1 was incubated with GST or GST–TAp63alpha fusion proteins. After incubation, GST or GST–TAp63alpha fusion proteins was recovered by glutathione-Sepharose beads, and bound materials were resolved by 10% SDS–PAGE (polyacrylamide gel electrophoresis) followed by autoradiography.

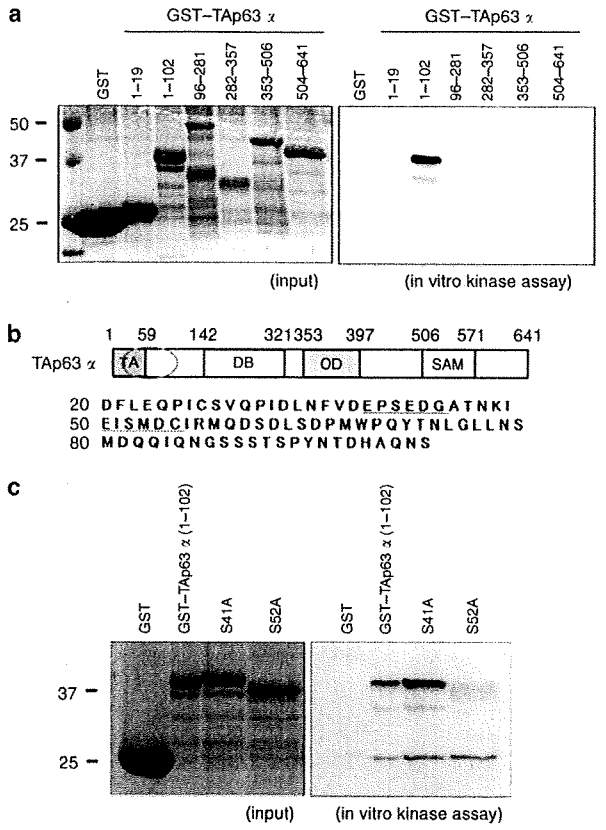

Figure 3 Plk1 directly phosphorylates Ser-52 of TAp63. (**a**) *in vitro* kinase assay. GST and GST-tagged TAp63alpha deletion mutants were incubated with the active form of Plk1 in the presence of [γ-^{32}P]ATP. The reaction mixtures were separated by SDS–PAGE (polyacrylamide gel electrophoresis) and subjected to autoradiography. (**b**) A sequence (D/E)*X*(S/T)ΦD/E) (where *X* is any amino acid and Φ is hydrophobic amino acid) was identified as a consensus motif for Plk1-dependent phosphorylation. According to the search for a putative phosphorylation site(s) targeted by Plk1 within the amino acid sequence of TAp63 (residues 20–96), related motifs, (39EPSEDG44 and 50EISMDC55), were in the NH2-terminal portion of TAp63alpha. (**c**) *in vitro* kinase assay. GST and GST-TA63alpha-(1–102)S41A, and GST-TA63alpha-(1–102)S52A were incubated with the active form of Plk1 in the presence of [γ-^{32}P]ATP. The reaction mixtures were separated by SDS–PAGE and subjected to autoradiography.

however, these phenomena were attenuated by co-transfection of Plk1, and KD Plk1 failed to attenuate it (Figure 5a). To study the molecular mechanism of the effect of Plk1-induced phosphorylation on the function of TAp63, we checked the protein stability of TAp63alpha in the presence of Plk1 or KD Plk1(K82M). As shown in Figures 5b and c, Plk1 clearly decreased the protein stability of TAp63alpha. On the other hand, KD Plk1(K82M) did not modify the protein stability of TAp63alpha. In addition, the Plk1-related degradation of TAp63 was not attenuated by a proteasome inhibitor MG132 (data not shown), consistent with the phenomenon in TAp73/Plk1 experiments (Koida *et al.*, 2008). These results suggest that Plk1 downregulates the protein stability of TAp63 by its phosphorylation through a proteasome-independent pathway and suppresses TAp63-induced cell death.

Expression of Plk1 and p63 in liver tumor cells

Earlier our laboratory reported that Plk1 is highly expressed in hepatoblastoma samples and that patients with a high expression of Plk1 showed significantly poorer prognosis than those with a low expression (Yamada *et al.*, 2004), indicating Plk1 involvement in carcinogenesis and its potential as a therapeutic target in liver cell malignancy. As the above results indicate the significance of Plk1/TAp63 in the regulation of cell death of cancer cells, we studied the expression level of Plk1 and p63 in liver tumor cell lines (Figure 6a). We used one hepatoblastoma cell line (Huh6) and five HCC cell lines. From the results of reverse transcription (RT)–PCR and western blotting, a considerable expression of Plk1 was observed in liver tumor cell lines. Also, TAp63 was expressed in all liver tumor cell lines and the deltaNp63 expression was observed in HLF and PLC/PRF/5 cells.

Significance of TAp63 in Plk1 knockdown-induced apoptosis of liver tumor cells

Next, we carried out a knockdown experiment of Plk1 using siRNA in liver tumor cells (Huh6, HLE and HLF cells). FACS analysis suggested that Plk1 knockdown induced an increase in the sub-G0/G1 fraction not only in p53 wild-type Huh6 cells but also in p53 mutant-type HLE cells (Figure 6b). As p53 is mutated in HLE cells, this suggested the significance of TAp63 and/or p73 in Plk1 knockdown-induced apoptosis of liver tumor cells; however, the sub-G0/G1 fraction did not increase in HLF cells. In both HLE and HLF cells, p53 was mutated, and TAp63 and p73 were considerably expressed, although the expression of deltaNp63 was detected only in HLF cells (Figure 6a and Supplementary data), suggesting the possible anti-apoptotic effect of deltaNp63 in Plk1 knockdown-induced apoptosis. Next, we studied the influence of Plk1 knockdown on p53 family downstream effectors in liver tumor cells by RT–PCR experiments (Figure 6c). Plk1 knockdown transactivated the p53 family downstream effectors $p21^{Cip1/WAF1}$, *GADD45* and *PUMA* in Huh6 cells, and $p21^{Cip1/WAF1}$, *14-3-3σ* and *PUMA* in HLE cells.

As a result of Plk1 single knockdown, we found significant TAp63 in Plk1 knockdown-induced apoptosis pathways. Next, we carried out double knockdown experiments of Plk1/TAp63 using HLE cells. Plk1 single knockdown increased cell death, but this was suppressed by double knockdown of Plk1/TAp63 (Figure 6d). Furthermore, we examined the influence of double knockdown of Plk1/TAp63 on the expression of p53 family downstream effectors by RT–PCR (Figure 6e). *PUMA*, *14-3-3σ* and $p21^{Cip1/WAF1}$ expression levels were increased by Plk1 single knockdown, and double knockdown of Plk1 and TAp63 successfully abolished the increase in p53 family downstream effectors by the single knockdown.

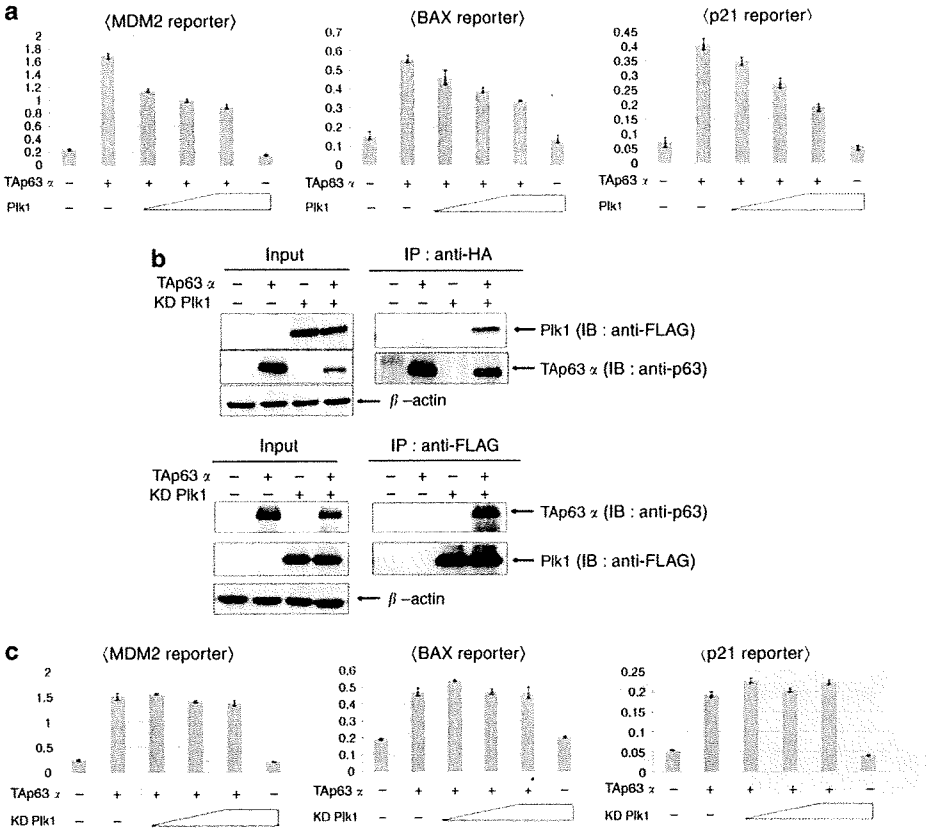

Figure 4 Plk1 represses TAp63-mediated transcriptional activation. (**a** and **c**) H1299 cells (5×10^4 cells) were co-transfected with a constant amount of TAp63alpha expression plasmid (25 ng), 100 ng of p53/p63-responsive luciferase reporter construct bearing $p21^{Cip1/WAF1}$, *BAX* or *MDM2* promoter and 10 ng of *Renilla* luciferase reporter plasmid (pRL-TK) in the presence or absence of increasing amounts of FLAG-Plk1 expression plasmid (**a**) or FLAG-Plk1(K82M) expression plasmid (**c**) (50, 100 and 200 ng). To standardize the amounts of plasmid DNA per transfection, pcDNA3 was added to yield 510 ng of plasmids. At 48 h after transfection, cells were lysed, and their luciferase activities were measured. Data were normalized and presented as mean values ± s.d. of three independent experiments. (**b**) Plk1(K82M) retains the ability to interact with TAp63 in cells. COS-7 cells were transiently transfected with FLAG-KD Plk1 and/or HA-TAp63 expression plasmids, immunoprecipitated with monoclonal anti-HA antibody (clone 3F10, Roche) and monoclonal anti-FLAG antibody (clone M2, Sigma), and immunoblotted with monoclonal anti-FLAG antibody and monoclonal anti-p63 antibody (clone 4a4) as indicated, to observe the interaction.

Possible role of Plk1/p63 in cancer stem cell fraction of liver tumor cells

Previous research showed that the involvement of Plk1 is crucial for the metaphase–anaphase transition. Plk1 mRNA and protein levels are coordinately regulated during cell-cycle progression and are highest in the mitotic phase (Winkles and Alberts, 2005; Eckerdt and Strebhardt, 2006). These observations suggested that Plk1 expression may be modest in the cancer stem cell fraction and that have a less significant role in cell death as cancer stem cells are generally accumulated in the Go/G1 phase (Zhou and Zhang, 2008). To examine expression levels of Plk1 and p63 in the cancer stem cell fraction, we carried out real-time PCR using the side population (SP) fraction and non-SP fraction of liver tumor cells. Surprisingly, the result suggested that both Plk1/p63 are highly expressed in the SP fraction compared with in the non-SP fraction (Figure 7a). Furthermore, the expression level of TAp63 was higher than that of deltaNp63 in the SP fraction of Huh7 cells, and almost equal to PLC/PRF/5 cells (Figure 7b). An analysis of the p63 downstream molecules in the SP and non-SP fraction indicated that p63 activities were repressed in the SP fraction except for the p21 activation in PLC/PRF/5 cells (Figure 7c), suggesting the possibility that p21 might be induced in a p53/TAp63-independent manner. These results suggest the considerable role of Plk1/p63 in the development of cancer stem cell-targeted therapy for liver tumor cells.

Discussion

Post-translational modification of p53 family members is a key phenomenon in their regulation (Shieh *et al.*, 1997); however, the regulation of p63 through post-translational modification has been studied only recently (Huang *et al.*, 2004; Ghioni *et al.*, 2005). From these studies, it has been suggested that p63 protein levels can change rapidly as a result of post-translational mod-

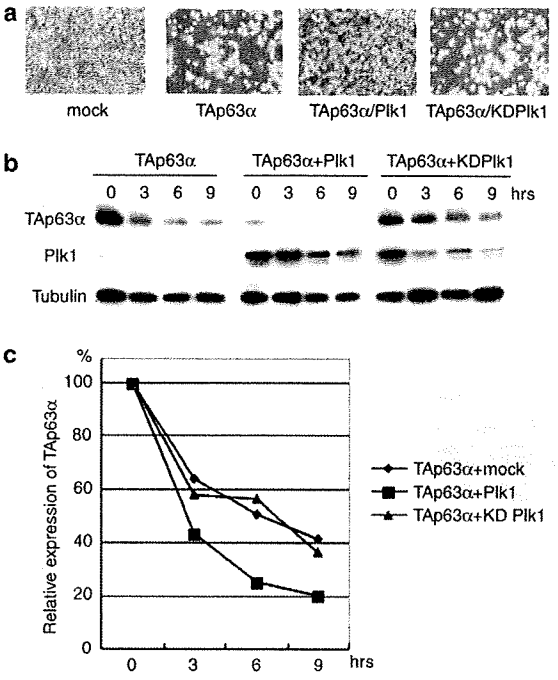

Figure 5 Plk1 downregulates the protein stability of TAp63 by its phosphorylation and suppresses TAp63-induced cell death. (**a**) H1299 cells were transfected with TAp63alpha alone or together with Plk1 or KD Plk1. At 24-h post-transfection, the cells were observed. (**b**) Decreased half-life of TAp63alpha in the presence of Plk1. Hep3B cells were transfected with TAp63lpha alone or together with Plk1 or KD Plk1. At 24-h post-transfection, the cells were treated with cycloheximide (50 μg/ml) and harvested at the indicated time points after the addition of cycloheximide. Cell lysates were analysed by SDS–PAGE (polyacrylamide gel electrophoresis) and immunoblotting. (**c**) Densitometric analysis of all TAp63alpha protein bands relative to tubulin was measured using NIH ImageJ software and plotted on a graph. The value of 0-h signals was indicated as 100%.

ification. At present, limited studies of the phosphorylation status of p63 have been reported (Westfall *et al.*, 2005; Suh *et al.*, 2006). DNA damage induces both the phosphorylation of p63 and its binding to p53 cognate DNA sites, and these events are linked to oocyte death (Suh *et al.*, 2006). TAp63 is constitutively expressed in female germ cells during meiotic arrest and is essential in the process of DNA-damage-induced oocyte death not involving p53. Furthermore, the phosphorylation of TAp63γ, but not deltaNp63γ, by IκB kinase β (IKKβ) was reported, although the exact amino acid residue for phosphorylation was not determined (MacPartlin *et al.*, 2008). The IKKβ-related phosphorylation of TAp63γ was also induced by γ-radiation. Upon ultraviolet radiation, deltaNp63α was phosphorylated at the ser-66/68 (in TAp63α, Ser-160/162) residues and led to ubiquitin-mediated degradation, suggesting that the protein stability of deltaNp63 is controlled by phosphorylation of different amino acid residues compared with that of TAp63 (Westfall *et al.*, 2005).

In this study, we reported that Plk1 directly interacts with p63 and the Ser-52 residue of TAp63 is phosphorylated by Plk1 (Figure 3). This Plk1-induced TAp63 phosphorylation might not to be related to the DNA-damage-induced phosphorylation of TAp63, as Plk1 was shown to be downregulated in response to DNA damage (Smits *et al.*, 2000; van Vugt *et al.*, 2001); however, the Ser-52 phosphorylation of TAp63 after DNA damage should be examined for the following reasons: (1) IKKβ-induced phosphorylation of TAp63 was shown in the TA domain of TAp63γ and was related to TAp63γ stabilization in response to γ-radiation (MacPartlin *et al.*, 2008) and (2) radiation-induced phosphorylation/activation of p63 in oocytes occurs in TAp63 but not in deltaNp63 (Suh *et al.*, 2006). Interestingly, the previously reported p63 phosphorylation was related to protein stabilization, upregulation of activity and induction of apoptotic cell death (Westfall *et al.*, 2005; Suh *et al.*, 2006). This study, however, clarified that phosphorylation by Plk1 results in protein degradation and suppression of the transcriptional activity of TAp63alpha (Figure 5b), consistent with the inactivation of transcriptional activity in p53 (Ando *et al.*, 2004) and p73alpha (Koida *et al.*, 2008). It can be noted that, this Plk1-related TAp63 degradation was affected by cell density of Hep3B cells (data not shown), suggesting that further analysis of p63 phosphorylation and its effect on degradation will be required in future.

The study of Ser-52 phosphorylation not only in DNA damage response but also in oncogene-related stimulation will contribute to understanding the exact role of Plk1-related tumorigenesis in many malignancies. Anti-phosphor-Ser-52 TAp63 antibody will be an indispensable tool for those studies and phosphorylation of Ser-52 among TAp63 isoforms, TAp63α/TAp63β/TAp63γ, should be addressed in various malignancies. Another interesting finding in our study is that both Plk1/p63 were highly expressed in the SP fraction of liver tumor cells compared with the non-SP fraction, although p63 downstream molecules were not induced in SP fraction except for p21 (Figure 7), suggesting that Plk1 has an important function in preventing apoptotic cell death in tumorigenesis through the inactivation of p53 family members in tumor-initiating cells; therefore, the functional interaction of this Plk1–p53 family protein appears to be a candidate for tumor-initiating cell-targeted therapy.

Despite strong and continuing emphasis on the involvement of the p53 family in tumorigenesis because of the tumor suppressive role of the founding member p53, it now seems evident that the remaining family members, p63 and p73, are highly involved in regulating the development of different tissues (Candi *et al.*, 2007). In particular, lines of evidence indicate that the main role of p63 lies in the regulation of epithelial development and, in particular, in the formation of the epidermis (Mills *et al.*, 1999; Yang *et al.*, 1999); however, the exact molecular regulation mechanism of TAp63/deltaNp63 transcriptional activities related to development and tumor suppression remains to be elucidated. Recently, several target genes of TAp63 in epithelial development have been identified, for example, IKKa/GATA-3 (Candi *et al.*, 2006), Jagged-1&-2 (Sasaki *et al.*,

2002), Hes-1/Hey-1&-2 (Nguyen *et al.*, 2006), K14 (Koster *et al.*, 2004) and p21 (Westfall *et al.*, 2003). We also reported that TAp63-dependent induction of growth differentiation factor 15 (GDF15) has a critical function in the regulation of keratinocyte differentiation (Ichikawa *et al.*, 2008). Investigation of the role of the Ser-52 phosphorylation of TAp63 in selective transactivation of these specific target genes will be an interesting research project to understand development regulation.

Furthermore, it was recently reported that Plk1 homozygous null mice were embryonic lethal and early Plk1−/− embryos failed to survive after the eight-cell stage. Immunocytochemistry studies showed that Plk1 null embryos were arrested outside the mitotic phase (Lu *et al.*, 2008). These observations suggest that the Plk1/p63 relationship may play an important role not only in later epithelial tissue organization but also in early embryonic development.

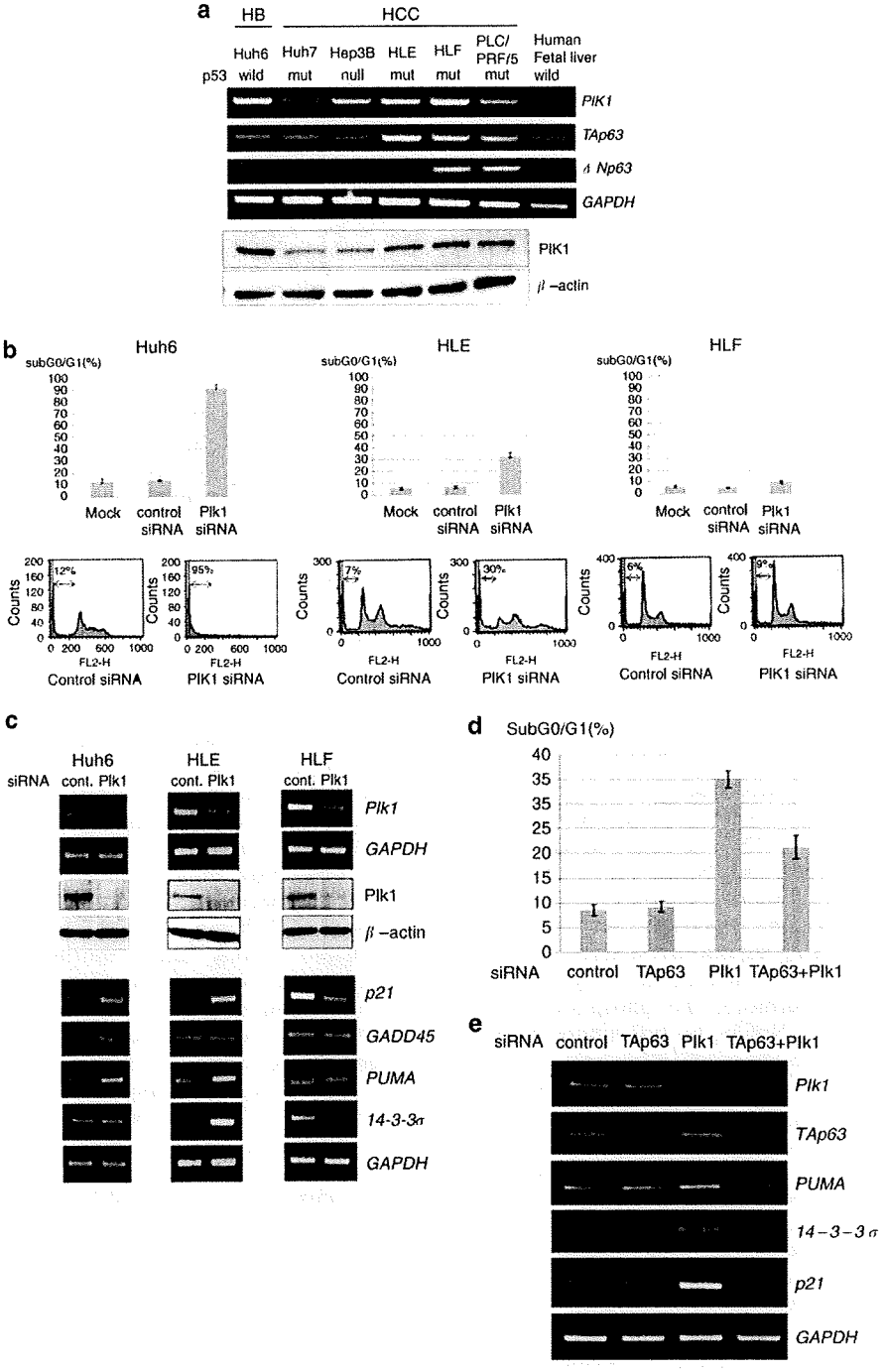

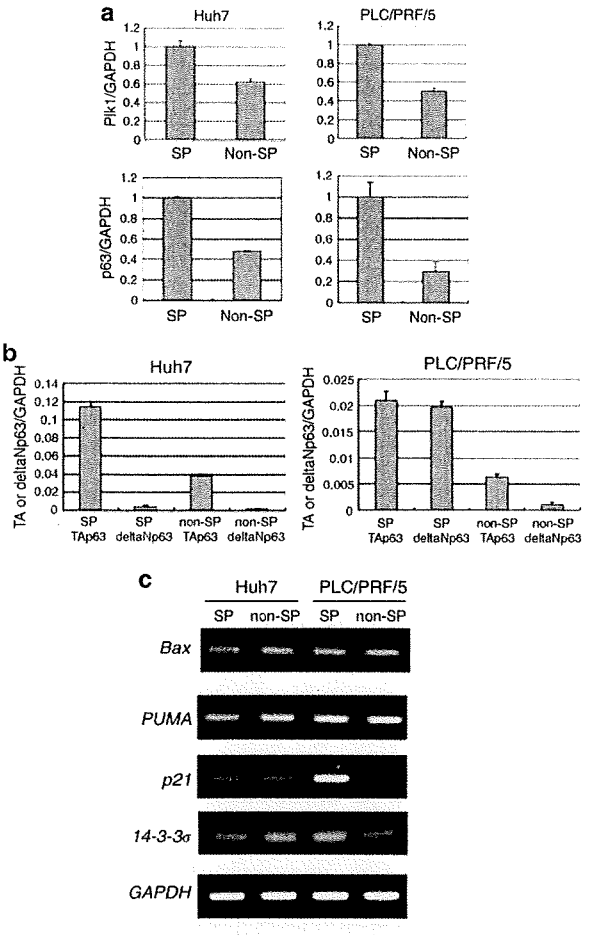

Figure 7 Possible role of Plk1/p63 in tumor-initiating cell fraction of liver tumor cells. (**a**) Using the side population (SP) fraction and non-SP fraction of liver tumor cells, expression levels of Plk1 and p63 were examined by real-time PCR analysis. Data were normalized and presented as the mean values ± s.d. of three independent experiments. (**b**) TAp63 and deltaNp63 expression levels in the SP fraction of liver tumor cells. Expression levels of TAp63 and deltaNp63 were examined by real-time PCR analysis. Data were normalized and presented as the mean ± s.d. of three independent experiments. (**c**) Semiquantitative reverse transcription (RT)–PCR analysis of the expression of *Bax*, *Puma*, *14-3-3σ* and *p21* in SP and non-SP cells.

Materials and methods

Cell culture

The African green monkey kidney cell line COS-7, human lung carcinoma cell line H1299, human hepatoblastoma cell line Huh6, HCC cell lines Huh7, Hep3B, HLE, HLF and PLC/PRF/5, and keratinocyte-like HaCaT cells were maintained in Dulbecco's modified Eagle's medium supplemented with 10% heat-inactivated fetal bovine serum (Invitrogen, Carlsbad, CA, USA), 50 μg/ml of penicillin and streptomycin each (Invitrogen). These cells were incubated at 37 °C in an atmosphere containing 5% CO_2.

RNA extraction and RT–PCR

Total RNA extraction, cDNA synthesis and semi-quantitative RT–PCR were carried out as described earlier (Koida *et al.*, 2008). The specific primers were indicated as supplements (Supplementary data). The expression of GAPDH (glyceraldehyde-3-phosphate dehydrogenase) was measured as an internal control.

SP analysis

Side population analyses were conducted as described earlier (Chiba *et al.*, 2006). We have studied the hepatocellular markers such as AFP (alpha-fetoprotein) or cytokeratin19 (CK19) of SP and non-SP cells that are obtained by sorting, and a large number of cells positive for both markers were observed in SP cells (Chiba *et al.*, 2006).

Quantitative real-time RT–PCR of Plk1 and TAp63

Polymerase chain reaction of TAp63 was carried out using TaqMan technology (Applied Biosystems, Foster City, CA, USA). Gene expression assay primer and probe mixes were used for TAp63 and GAPDH (assay IDs: Hs00186613_m1 and 4310884E, respectively), and reactions were carried out according to the manufacturer's protocol. Polymerase chain reaction of Plk1 was carried out using SYBR Green technology (Takara Bio, Otsu, Shiga, Japan). PCR was carried out using an ABI Prism 7700 Sequence Detection System (Perkin-Elmer/Applied Biosystems, Carlsbad, CA, USA). Primers were indicated in Supplementary data.

Protein extraction and western blot analysis

Extraction of cellular proteins, protein concentration analysis, SDS–PAGE, protein transfer and western blot analysis were carried out as described in Supplementary data.

Figure 6 Plk1 knockdown transactivates p53 family downstream effectors and induces apoptotic cell death. (**a**) Semiquantitative reverse transcription (RT)–PCR and western blotting of Plk1 and p53 family in hepatoblastoma and hepatocellular carcinoma cell lines. (**b**) FACS analysis of liver tumor cells subjected to small interfering RNA (siRNA)-mediated knockdown of endogenous Plk1. Cells were transfected with 10 nM of control siRNA or Plk1 siRNA. At 48 h after transfection, both floating and attached cells were collected by low-speed centrifugation. The cells were then stained with propidium iodide (50 μg/ml) in the presence of 50 μg/ml of RNase A for 30 min at room temperature. The DNA content indicated by propidium iodide staining was analysed using a FACSCalibur flow cytometer. (**c**) RT–PCR analysis of siRNA-mediated knockdown of endogenous Plk1 in liver tumor cells. Cells were transfected with 10 nM of control siRNA or Plk1 siRNA. At 48 h after transfection, total RNA was prepared and analysed for expression levels of $p21^{Cip1/WAF1}$, *GADD45*, *PUMA* and *14-3-3σ*. Amplification of *GAPDH* serves as an internal control. (**d**) FACS analysis of siRNA-treated cells. HLE cells were transfected with TAp63 siRNA and/or Plk1 siRNA. To standardize the amounts of siRNA per transfection, control siRNA was added to yield 15 nM of siRNA. At 48 h after transfection, both floating and attached cells were collected by low-speed centrifugation. Cells were then stained with propidium iodide (50 μg/ml) in the presence of 50 μg/ml of RNase A for 30 min at room temperature. The DNA content indicated by propidium iodide staining was analysed using a FACSCalibur flow cytometer. (**e**) RT–PCR analysis of siRNA-treated cells. HLE cells were transfected with TAp63 siRNA and/or Plk1 siRNA. To standardize the amounts of siRNA per transfection, control siRNA was added to yield 15 nM of siRNA. At 48 h after transfection, total RNA was prepared and analysed for expression levels of $p21^{Cip1/WAF1}$, *PUMA* and *14-3-3σ*. Amplification of *GAPDH* serves as an internal control.

Immunoprecipitation and western blot analysis
For the immunoprecipitation of Plk1 and p63, COS-7 cells were transiently transfected with 2 μg of the expression plasmids for FLAG-Plk1 and or HA-TAp63alpha using Lipofectamine 2000 Transfection Reagent (Invitrogen). Protein extraction was carried out as described earlier. The extracts were incubated with the monoclonal anti-FLAG (clone M2, Sigma, St Louis, MO, USA) or monoclonal anti-HA antibody (clone 3F10, Boehringer Roche, Mannheim, Germany) at 4 °C for 8 h. Immunocomplexes were precipitated with protein G-Sepharose beads at 4 °C for 30 min, which were then pelleted by centrifugation at 15 000 *g* for 5 min. The precipitates were washed with lysis buffer three times at 4 °C, resuspended in 30 μl of SDS sample buffer and treated at 100 °C for 5 min. Proteins were then resolved by 8% SDS–PAGE, and transferred onto Immobilon-P membranes (Millipore, Bedford, MA, USA). The protein complex was detected by western blot analysis using monoclonal anti-FLAG or monoclonal anti-p63 antibodies.

GST pull-down assay
cDNA fragments encoding the indicated deletion mutants of TAp63alpha were generated by a PCR-based strategy, and subcloned into GST fusion protein expression plasmid pGEX-4T-1 (GE Healthcare, Piscataway, NJ, USA). GST and GST–TAp63alpha fusion proteins were expressed and purified using glutathione-Sepharose beads (Amersham Biosciences). FLAG-Plk1 was radiolabeled *in vitro* using the TNT Quick Coupled transcription/translation system (Promega, Madison, WI, USA) in the presence of [^{35}S]methionine and incubated with GST or GST–TAp63alpha deletion mutants at 4 °C for 2 h. After the addition of 30 μl glutathione-Sepharose beads to the reaction mixture, incubation was continued at 4 °C for 1 h. The beads were collected by centrifugation and washed three times with binding buffer containing 50 mM Tris-HCl (pH 7.5), 150 mM NaCl, 0.1% Nonidet P-40 and 1 mM EDTA. The ^{35}S-labeled-bound proteins were eluted using 2 × SDS sample buffer and separated by 10% SDS–PAGE. After electrophoresis, the gel was dried and exposed to X-ray film with an intensifying screen.

Flow cytometry
After transfection, both floating and attached cells were collected by low-speed centrifugation and washed in phosphate-buffered saline. The cells were then stained with propidium iodide (50 μg/ml) in the presence of 50 μg/ml of RNase A for 30 min at room temperature. The DNA content indicated by propidium iodide staining was analysed using a FACSCalibur flow cytometer (BD Biosciences, San Jose, CA, USA).

Luciferase reporter assay
Luciferase reporter assay was carried out as described earlier (Koida *et al*., 2008). Each experiment was carried out at least three times in triplicate.

In vitro *kinase assay*
To identify the possible Ser residue(s) of TAp63alpha that could be phosphorylated by Plk1, we carried out *in vitro* kinase assay according to the previous report (Koida *et al*., 2008). In brief, GST–TAp63alpha-(1–102), GST-S41A and GST-S52A were incubated with the active form of Plk1 (cat no. CY-E1163, CycLex, Nagano, Japan) in the presence of 10 μCi of [γ-^{32}P]ATP (~6000 Ci/mmol, GE Healthcare) in 40 μl of kinase buffer (40 mM HEPES (4-(2-hydroxyethyl)-1-piperazineethanesulfonic acid), 10 mM $MgCl_2$, 1 mM dithiotreitol and 3 mM $MnCl_2$). Reactions were incubated at 30 °C for 30 min and terminated by the addition of Laemmli SDS sample dilution buffer. The reaction mixtures were separated by SDS–PAGE and subjected to autoradiography.

RNA interference
To knockdown endogenous Plk1, TAp63 and p73, cells were transiently transfected with the chemically synthesized siRNA targeting Plk1, TAp63 and p73 or with the control siRNA using Lipofectamine RNAiMAX (Invitrogen) according to the manufacturer's recommendations. Total RNA and whole-cell lysates were prepared 48 h after transfection. The specific sequences were as follows: Plk1, 5′-AACCAGUGGUUCGAGAGACAG-3′; TAp63, 5′-GAUGGUGCGACAAACAAGA-3′; and p73, 5′-CGGAUUCCAGCAUGGACGU-3′. Selected siRNA sequences were submitted to a BLAST search against the human genome sequence to ensure specificity. *Silencer* Negative Control #1 siRNA (Ambion, Austin, TX, USA) was used as control siRNA.

Construction of the deletion mutants of Plk1
For construction of the deletion mutants of Plk1, pcDNA3-FLAG-*Plk1* was digested with *Bam*HI, *Bam*HI/*Bst*XI and *Bam*HI/*Nco*I for the fragments encoding amino acid residues 1–401, 1–329 and 1–98, respectively. These fragments were purified from agarose gels, filled in the overhangs with Klenow enzyme and then inserted in-frame into enzymatically modified *Bam*HI and *Xho*I sites of the pcDNA3-FLAG expression plasmid to obtain pcDNA3-FLAG-*Plk1*-(1–401), pcDNA3-FLAG-*Plk1*-(1–329), and pcDNA3-FLAG*Plk1*-(1–98), respectively. DNA sequencing confirmed the authenticity of the expression plasmids before transfection.

Acknowledgements

We thank K Sakurai for technical assistance and Daniel Mrozek, Medical English Service, for editorial assistance. This work was supported, in part, by a grant-in-aid from the Ministry of Health, Labor, and Welfare for Third Term Comprehensive Control Research for Cancer; a grant-in-aid for Cancer Research (20-13) from the Ministry of Health, Labor, and Welfare of Japan; and a grant-in-aid from the Ministry of Education, Culture, Sports, Science and Technology, Japan.

References

Ando K, Ozaki T, Yamamoto H, Furuya K, Hosoda M, Hayashi S *et al*. (2004). Polo-like kinase 1 (Plk1) inhibits p53 function by physical interaction and phosphorylation. *J Biol Chem* **279**: 25549–25561.

Blandino G, Dobbelstein M. (2004). p73 and p63: why do we still need them? *Cell Cycle* **3**: 886–894.

Bruix J, Llovet JM. (2002). Prognostic prediction and treatment strategy in hepatocellular carcinoma. *Hepatology* **35**: 519–524.

Candi E, Dinsdale D, Rufini A, Salomoni P, Knight RA, Mueller M *et al*. (2007). TAp63 and DeltaNp63 in cancer and epidermal development. *Cell Cycle* **6**: 274–285.